Phosphate starvation-induced CORNICHON HOMOLOG 5 as endoplasmic reticulum cargo receptor for PHT1 transporters in *Arabidopsis*

Chang-Yi Chiu,[a], Cheng-Da Tsai,[a], Jhih-Yi Wang,[a], Ming-Hsuan Tsai,[a], Alastair J. McGinness,[b], Hui-Fang Lung,[a], Satomi Kanno,[c], Verena Kriechbaumer,[b], Tzu-Yin Liu,[a,d,1]

[a]Institute of Bioinformatics and Structural Biology, College of Life Sciences and Medicine, National Tsing Hua University, Hsinchu 30013, Taiwan.
[b]Endomembrane Structure and Function Research Group, School of Biological and Medical Sciences, Oxford Brookes University, Headington, Oxford OX3 0BP, UK
[c]Institute for Advanced Research, NAIAS, Nagoya University, Fro-cho, Chikusa-ku, Nagoya, Japan.
[d]Department of Life Science, College of Life Sciences and Medicine, National Tsing Hua University, Hsinchu 30013, Taiwan.

[1]Address correspondence to tzliu@life.nthu.edu.tw
Institute of Bioinformatics and Structural Biology, College of Life Sciences and Medicine, National Tsing Hua University, Hsinchu 30013, Taiwan
Tel: +886 3 574-2096; Fax: +886 3 571-5934

Running title: CNIH5 facilitates ER export of PHT1 transporters

Synopsis: Phosphate starvation-induced CNIH5 acts as an ER cargo receptor of PHT1 transporters in *Arabidopsis*, enhancing their plasma membrane targeting and phosphate uptake.

The author responsible for distribution of materials integral to the findings presented in this article in accordance with the policy described in the Instructions for Authors (https://academic.oup.com/plcell/pages/General-Instructions) is: Tzu-Yin Liu (tzliu@life.nthu.edu.tw)

Key words: CORNICHON HOMOLOG, ER cargo receptor, phosphate starvation, phosphate transporter, ER exit sites (ERES)

ABSTRACT

Phosphate (Pi) is essential for plant growth and is acquired by the plasma membrane (PM) PHOSPHATE TRANSPORTER 1 proteins (PHT1s). Enhancing the abundance of PHT1s at the cell surface under Pi limitation thus ensures plant productivity and sustainable agriculture. CORNICHON HOMOLOG proteins (CNIHs) are conserved eukaryotic cargo receptors that mediate the selective endoplasmic reticulum (ER) export of membrane proteins. We identified the *Arabidopsis thaliana CNIH5* (*AtCNIH5*) as a Pi starvation-inducible gene preferentially expressed in the outer root cell layers above the meristem. *At*CNIH5 co-localizes to the *At*SAR1A/*At*SEC16A/*At*SEC24A-labeled ER exit sites and interacts with *At*PHT1;1 and PHOSPHATE TRANSPORTER TRAFFIC FACILITATOR1 (*At*PHF1). Loss of *AtCNIH5* confers reduced shoot Pi levels and decreased *At*PHT1s but increased *At*PHF1. The root hair and the epidermis within the transition/elongation zone of the *cnih5* mutant display a lower PM targeting efficiency of *At*PHT1;1. Moreover, dysfunctional *At*CNIH5 exerts a suppressive effect on the growth of *phf1* and alleviates Pi toxicity in the Pi overaccumulator *pho2*. However, the *in vivo* protein–protein interaction and degradation assays indicated that *At*CNIH5 is not a direct target of *At*PHO2. Our findings unveil that low Pi-responsive *At*CNIH5 interplays with *At*PHF1 to promote the PM targeting of *At*PHT1s in a cell type-dependent manner.

INTRODUCTION

Membrane trafficking that dictates the plasma membrane (PM) proteins in reaching their destination is intimately linked with plants' plasticity to changing environments and, thus, crucial for plant growth and fitness under adverse conditions. Among the endoplasmic reticulum (ER) accessory proteins involved in membrane trafficking, CORNICHON HOMOLOGUE (CNIH) proteins are responsible for the selective export of membrane cargoes to the Golgi or post-Golgi compartments by cycling between the ER and the Golgi (Powers and Barlowe, 1998; Harmel et al., 2012). They are conserved in eukaryotes and presumably harbor three membrane-spanning α-helixes with the N-terminus towards the cytoplasm (Rosas-Santiago et al., 2015). The *Drosophila* cornichon is the first identified CNIH that promotes the ER export of the transforming growth factor α (TGFα)-like growth factor to the oocyte surface during oogenesis (Roth et al., 1995; Bökel et al., 2006). In the budding yeast *Saccharomyces cerevisiae*, the systematic genetic manipulations combined with automated microscopy screening uncovered that *Sc*CNIH/Erv14 serves as an ER cargo receptor of about 40 membrane cargoes with diverse functions, including proteins involved in transport, budding, sporulation, and cell wall synthesis (Powers and Barlowe, 1998; Powers and Barlowe, 2002; Nakanishi et al., 2007; Herzig et al., 2012; Pagant et al., 2015; Zimmermannová et al., 2019). Of note, yeast cells lacking Erv14 showed normal PM localization of the K^+-importer Trk2 yet mistargeting its paralog Trk1, despite that Trk2 is nearly 55% identical to Trk1 (Zimmermannová et al., 2019), suggesting a regulatory mechanism operating in the cargo selectivity of CNIHs. For instance, Erv14 employs multiple modes of cargo binding to meet the different requirements of various cargo proteins. It simultaneously binds to the membrane cargo and the coat protein complex II (COPII) subunit Sec24, thus incorporating the membrane cargo into the COPII carriers (Powers and Barlowe, 1998; Powers and Barlowe, 2002; Pagant et al., 2015). Similarly, Sec24 was reported to recognize two signals to efficiently drive the ER exit of client proteins, one on membrane cargoes and the other on Erv14 (Pagant et al., 2015).

Despite plant CNIH proteins (CNIHs) being less functionally characterized, they seem to have a similar role as their yeast counterpart. The moss (*Physcomitrium patens*) *Pp*CNIH2 was identified as a specific cargo receptor of the auxin efflux transporter homolog PINA for

its polar localization in protonema cells (Yáñez-Domínguez et al., 2023). The rice (*Oryza sativa*) *Os*CNIH1 was shown to mediate the Golgi targeting of the sodium transporter *Os*HKT1;3 (Rosas-Santiago et al., 2015). Moreover, overexpression of the pumpkin (*Cucurbita moschata* var. Rifu) *Cm*CNIH1 improves the salt tolerance by regulating the PM localization of the sodium-selective transporter *Cm*HKT1;1 (Wei et al., 2023). Based on the PANTHER classification (http://www.pantherdb.org/), *Arabidopsis thaliana* CNIH1 (*At*CNIH1) and *Os*CNIH2 are grouped into the same subfamily as the yeast Erv14 and its paralog Erv15; *At*CNIH2, *At*CNIH4, and *Os*CNIH1 belong to the same subfamily; *At*CNIH3 and *At*CNIH5 (AT4G12090) are *Brassicaceae*-specific CNIH paralogs. The *Arabidopsis cnih1*, *cnih4*, and *cnih1/4* double mutants were shown to exhibit reduced Ca^{2+} fluxes in the pollen tube tip due to the impaired targeting of glutamate receptor-like channels (GLRs) (Wudick et al., 2018). Furthermore, the patch-clamp analysis of mammalian COS-7 cells expressing *At*GLR3.3 together with *At*CNIH1 and *At*CNIH4 displayed a current two-fold relative to those co-expressing *At*GLR3.3 with *At*CNIH1 or *At*CNIH4 alone, indicating that the formation of *At*CNIH oligomers potentially imposes an additional layer of regulation on cellular Ca^{2+} homeostasis (Wudick et al., 2018). Therefore, by modulating the trafficking of various transporters along the secretory pathway, the plant CNIH family can regulate various ion homeostasis.

Phosphate (Pi) is known to be one of the most limiting mineral nutrients for plant growth and productivity. Because of its chemical properties, Pi is mostly immobilized in the soil, and its bioavailability is poor (Manning, 2008). To adapt to the low Pi availability, plants utilize a series of strategies, including enhancing Pi acquisition by the PM-localized PHOSPHATE TRANSPORTER 1 (PHT1) family (Poirier and Bucher, 2002; Młodzińska and Zboińska, 2016). In *Arabidopsis*, *At*PHT1;1 and *At*PHT1;4 are responsible for up to 75% of Pi uptake under a wide range of Pi concentrations and thus play dominant roles in Pi acquisition (Karthikeyan et al., 2002; Mudge et al., 2002; Misson et al., 2004; Shin et al., 2004; Ayadi et al., 2015). Under Pi repletion, *AtPHT1;1* shows a robust gene expression in the root hair-producing trichoblast and is the most abundant member (Karthikeyan et al., 2002; Mudge et al., 2002; Ayadi et al., 2015). In response to low Pi, *AtPHT1;1* is modestly induced, mainly in the root epidermis, cortex, and root hair, and is detectable throughout the

lateral root cap, whereas *AtPHT1;4* is highly induced (Karthikeyan et al., 2002; Mudge et al., 2002). Besides the low Pi induction of *PHT1* genes at the transcriptional level, the trafficking of PHT1 proteins (PHT1s) to the PM is also under constant surveillance. The ER exit of PHT1s requires PHOSPHATE TRANSPORTER TRAFFIC FACILITATOR1 (PHF1), an ER accessory protein sharing sequence homology with the small GTPase SAR1 guanine nucleotide exchange factor (GEF) SEC12 but missing the key catalytic residues required for the GEF activity (González et al., 2005). Dysfunction of *At*PHF1 specifically impairs Pi uptake by hampering the PM targeting of PHT1s, leading to a reduced abundance of PHT1s at the PM and a lower cellular Pi level, thereby activating Pi starvation-responsive (PSR) genes (González et al., 2005; Bayle et al., 2011). In rice, the phosphorylation status of the C-terminus of PHT1s affects their interaction with PHF1, and thus the ER exit of PHT1s (Chen et al., 2015; Yang et al., 2020). In addition, the turnover of PHT1s relies on the vacuolar degradation mediated either by the ENDOSOMAL SORTING COMPLEXES REQUIRED FOR TRANSPORT (ESCRT) III-related component (Cardona-López et al., 2015) or the ubiquitin E2 conjugase PHOSPHATE2 (PHO2) and/or the ubiquitin E3 ligase NITROGEN LIMITATION ADAPTATION (NLA) (Huang et al., 2013; Lin et al., 2013; Park et al., 2014). As a result, defective PHO2 or NLA confers Pi overaccumulation in plants due to increased accumulation of PHT1s (Huang et al., 2013; Lin et al., 2013).

Previous transcriptome profiling has uncovered *AtCNIH5* as a Pi starvation-induced gene with unknown implications (Müller et al., 2007; Liu et al., 2016). The membrane proteomics analysis of *Arabidopsis pho2* root also showed a significant increase of *At*CNIH5 along with a higher level of *At*PHT1;1–1;4 and *At*PHF1 (Huang et al., 2013). Although it remains to be determined whether *At*CNIH5 is a direct target of *At*PHO2, when querying a yeast split-ubiquitin-based *Arabidopsis* interactome database (*At*CNIH5 not included), we found that *At*CNIH1 interacts with *At*PHT1;9 and *At*PHF1 (Jones Alexander et al., 2014). These data prompted us to speculate that Pi starvation-induced *At*PHF1, *At*CNIH5, and *At*PHT1s are genetically and functionally linked. We were thus curious whether *At*CNIH proteins (*At*CNIHs), particularly *At*CNIH5, are involved in the regulatory mechanism for the post-ER trafficking of *At*PHT1s. In this study, we characterized *AtCNIH5* as the sole *AtCNIH* gene induced by Pi starvation in the outer root cell layers. We showed that in agro-infiltrated *N.*

benthamiana leaves, the fluorescent-tagged *At*CNIH5 is ER-localized and closely associated with the ER exit sites (ERES) markers *At*SAR1A, *At*SEC16A, and *At*SEC24A. We also confirmed the interaction of *At*CNIH5 with *At*PHT1;1 and *At*PHF1 using the *in-planta* split-GFP complementation, the yeast split-ubiquitin, and the co-immunoprecipitation (co-IP) assays. The *cnih5* T-DNA insertion mutant exhibits reduced shoot Pi levels, decreased amount of *At*PHT1s, increased *At*PHF1 accumulation, and impaired PM localization of split-GFP tagged-*At*PHT1;1 in the epidermis of the root transition/elongation zone and the root hair. The characterization of *cnih1/5*, *cnih3/5,* and *cnih4/5* double mutants further suggested that *At*CNIH5 is the primary *At*CNIH member regulating the cellular Pi homeostasis at the seedling stage. However, at an older growth stage, other *At*CNIH members may participate in this process. In addition, our genetic studies suggest that dysfunctional *At*CNIH5 exerts an additive suppressive effect on the growth of *phf1* and alleviates the Pi toxicity of the Pi overaccumulator *pho2*, supporting a role for *At*CNIH5 in regulating Pi homeostasis. Nevertheless, neither *At*CNIH5 interacts with *At*PHO2 *in planta*, nor does the transient expression of *At*PHO2 downregulate the expression of *At*CNIH5, arguing against *At*CNIH5 as a direct target of the *At*PHO2 regulatory module. Overall, our findings demonstrate that loss of *AtCNIH5* leads to a lower PM targeting efficiency of *At*PHT1s in a cell-type-dependent manner and reveal *At*CNIH5 as a *bona fide* ER cargo receptor that interplays with *At*PHF1 to ensure proper and efficient trafficking of *At*PHT1s to the cell surface.

RESULTS

*At*CNIH5 is induced by Pi deficiency preferentially in the outer root cell layers

To corroborate the responsiveness of *AtCNIH5* to Pi starvation, we examined by quantitative reverse transcription PCR (RT-qPCR) the transcript expression of all the *AtCNIH* genes except *AtCNIH2*, whose expression was barely detectable (Liu et al., 2016). Under Pi-repleted conditions, the expression of *AtCNIH5* was relatively low in the seedling; however, it remarkedly increased in both the shoot and root following Pi starvation (**Fig. 1A**). In contrast, *AtCNIH1*, *AtCNIH3*, and *AtCNIH4* were upregulated by nitrogen (N) deprivation (**Fig. 1A**). We analyzed the spatial expression pattern of *AtCNIH5* using promoter: *uidA* (a gene encoding β-glucuronidase or GUS) fusion lines. Under full-nutrient conditions, the

promoter activity of *AtCNIH5* was found in the trichomes and the vascular tissues of the shoot (**Fig. 1B**). In the primary root, the expression of *AtCNIH5* was absent in the root cap and meristem but strongly expressed in the stele of the transition/elongation and the differentiation/maturation zones (**Fig. 1B**). In the lateral root, *AtCNIH5* was also expressed in the vascular tissues and detectable in the columella (**Fig. 1B**). Interestingly, the promoter activity of *AtCNIH5* was markedly elevated in the outer cell layers of the primary root following Pi deprivation (**Fig. 1B**). In comparison, the promoter activity of *AtCNIH1*, *AtCNIH3*, and *AtCNIH4* was restricted to the vascular tissues of shoot and root of the primary root but present in the columella of the lateral root (**Supplementary Fig. S1**). Characterization of *AtCNIH5pro*: GFP fusion lines at the young seedling stage recapitulated that, irrespective of Pi regimes, *AtCNIH5* is expressed in the transition/elongation and differentiation/maturation zones of the primary root, including the cortex, epidermis, and root hairs (**Supplementary Fig. S2**). Collectively, the expression of *AtCNIH5* is enhanced by Pi starvation and its promoter activity is upregulated by low Pi in the outer root cell layers, including the root hairs.

_At_CNIH5 resides both at the ER and ERES

Previous studies of the pollen-specific expression of *At*CNIHs showed their distribution at the ER (Wudick et al., 2018). Furthermore, RFP-*At*CNIH4 could be detected at the pollen tube's PM and colocalized with the ERES marker *At*SEC24A (Wudick et al., 2018). To examine the subcellular distribution of *At*CNIH5 in other tissues, we generated the construct encoding UBQ10 promoter-driven β-estradiol-inducible *At*CNIH5 tagged with the 10th β-strand of GFP (S10-*At*CNIH5) for transient expression. In *N. benthamiana* leaves, the split-GFP self-complementation allows live-cell imaging of S10-tagged fusion proteins in the presence of the detector S11-GFP1–9 (Liu et al., 2018; Liu, 2021). The distribution of S10-*At*CNIH5 showed a typical ER-network pattern when co-expressed with the cytosolic S11-GFP1–9 (**Fig. 2A**), supporting that the N-terminus of *At*CNIH5 is in the cytoplasm. While S10-*At*CNIH5 colocalized with the ER-luminal marker mCherry-HDEL, the mCherry-*At*CNIH5-labeled punctate structures distributed on the ER tubules and sheet rims and were closely associated with the ERES marker *At*SEC16A/MAG5 (Takagi et al., 2013) (**Fig. 2A**).

Taking advantage of high-resolution confocal microscopy, we measured the distance between the red fluorescence protein-tagged *At*CNIH5 and the *cis*-Golgi marker MNS1 (Liebminger et al., 2009) and the three ERES markers *At*SAR1A-GFP, GFP-*At*SEC16A, and GFP-*At*SEC24A. Our results demonstrated that RFP-*At*CNIH5 and mCherry-*At*CNIH5 significantly colocalized with the tested ERES markers but not with the *cis*-Golgi marker (**Fig. 2B** and **2C**).

To validate the subcellular localization of *At*CNIH5 in stable lines, we generated the transgenic plants expressing RFP-*At*CNIH5 under the cauliflower mosaic virus (CaMV) 35S promoter. Although RFP-*At*CNIH5 signals displayed intracellular patterns in the root cells, the plants exhibited abnormal root development (**Supplementary Fig. S3**). Additionally, we used *cnih5* as the genetic background to obtain transgenic plants carrying the genomic sequence of *At*CNIH5 translationally in-frame with GFP (*AtCNIH5pro*: GFP-*AtCNIH5*). Compared to the *cnih5* control, three independent lines had increased shoot biomass but exhibited decreased shoot Pi levels (**Supplementary Fig. S4**). The signals of GFP-*AtCNIH5* were also overall fain; however, we observed the reticular and puncta patterns in the hair and epidermal cells of the Pi-starved root (**Fig. 2D**), suggesting that the ER and ERES localization of *At*CNIH5 observed in *N. benthamiana* leaves was unlikely an overexpression artifact.

_At_CNIH5 interacts with _At_PHT1s and _At_PHF1

The yeast split ubiquitin-based interactome revealed the interaction of *At*CNIH1 with *At*PHT1;9 and *At*PHF1 (Jones Alexander et al., 2014), prompting us to test whether *At*CNIH5 also interacts with *At*PHT1s and *At*PHF1. Considering the expression of *AtCNIH5* and *AtPHT1;1* mainly in the root epidermis, we selected *At*PHT1;1 to represent *At*PHT1s in this study. In agro-infiltrated *N. benthamiana* leaves, S10-*At*CNIH5 interacted with the 11th β-strand of sfGFP-tagged *At*PHT1;1 (*At*PHT1;1-S11), as manifested by the reconstituted GFP signals in the presence of the cytosolic GFP1–9 (Liu et al., 2018; Liu, 2021) (**Fig. 3A**). Due to the same putative membrane topology shared by *At*CNIH5 and *At*PHF1, the tripartite split-GFP complementation method is not suitable for detecting the interaction between these two proteins. We then exploited the yeast ubiquitin-based system (SUS) to examine the interaction between *At*CNIH5 and *At*PHF1 as well as to verify the interaction between

*At*CNIH5 and *At*PHT1s. The results of the nutrient selection and the LacZ β-galactosidase assays suggested that *At*CNIH5 interacted with *At*PHF1, *At*PHT1;1, and *At*PHT1;4 (**Fig. 3B**). In addition, we performed co-immunoprecipitation using the *Arabidopsis* transgenic plants harboring the genomic GFP-*At*CNIH5 (*AtCNIH5pro*: GFP-*AtCNIH5/cnih5*) or the free GFP under the UBQ10 promoter. Although the cytosolic GFP was nearly 20-fold more abundant relative to GFP-*AtCNIH5* in the root low-speed pellet (LSP) membrane fraction, the amount of the endogenous *At*PHT1;1/2/3 immunoprecipitated with GFP-*AtCNIH5* was increased by 2.9-fold relative to that of GFP (**Fig. 3C**). These results supported our presumption that *At*CNIH5 acts as an ER cargo receptor of *At*PHT1s to assist their ER exit.

Loss of *AtCNIH5* confers reduced Pi levels, *At*PHT1s accumulation, and Pi uptake

To determine the physiological role of *At*CNIH5, we grew WT and *cnih5* mutants under different Pi regimes. Regardless of Pi status, the shoot and root fresh weight (FW) of *cnih5* mutants showed no differences from that of WT (**Fig. 4A**). By contrast, the shoot Pi level of *cnih5* diminished to 10–20% of WT under Pi sufficiency (**Fig. 4B**). We could rescue the lower shoot Pi concentrations in *cnih5* by introducing the genomic construct encoding *At*CNIH5 (*AtCNIH5pro*: *AtCNIH5*) (**Supplementary Fig. S4**), reinforcing that the reduced Pi accumulation in *cnih5* was attributed to the non-functional *cnih5* allele. Additionally, the lower shoot Pi level in *cnih5* did not cause the upregulation of Pi starvation-induced genes in the root (**Supplementary Fig. S5**). The primary root length of *cnih5* was also similar to that of WT (**Supplementary Fig. S5**). The lateral root density was increased in *cnih5* under Pi-sufficient conditions (**Supplementary Fig. S5**). In contrast, the root hair length and density of *cnih5* were 10% shorter and 40% higher, respectively, than that of WT under Pi-deficient conditions (**Supplementary Fig. S5**).

To evaluate whether *At*PHT1s accounts for the decreased Pi levels in *cnih5*, we examined the expression level of *At*PHT1;1/2/3 and *At*PHT1;4 proteins, which are the prominent *At*PHT1 members involved in Pi uptake (Shin et al., 2004; Ayadi et al., 2015). We assume that defective *At*CNIH5 would hamper the ER export of *At*PHT1 transporters, thus diminishing the steady-state level of *At*PHT1s due to protein quality control. As the previous RNA-seq analysis suggested *AtCNIH4* as the most abundant *AtCNIH* gene member (Liu et

al., 2016), we included *cnih4* mutants for comparison. Under Pi sufficiency, the amount of *At*PHT1;1/2/3 and *At*PHT1;4 in the total root proteins was indistinguishable among WT, *cnih4*, and *cnih5*; however, under Pi deficiency, these proteins were decreased in *cnih5* by 20–25% as compared to WT (**Supplementary Fig. S6**). After enrichment of root membrane proteins, a 50% decrease of *At*PHT1;1/2/3 was detected in *cnih5* under both Pi regimes (**Fig. 4C**). The level of *At*PHT1;4 was also reduced by 40% in the root membrane proteins of *cnih5* as compared with the corresponding WT controls (**Fig. 4C**). Notably, the expression of *At*PHT1;1/2/3 was restored to the WT-like level in the *cnih5* complemented lines carrying the genomic *AtCNIH5pro*: *AtCNIH5* or the genomic *AtCNIH5pro*: GFP-*AtCNIH5* constructs (**Supplementary Fig. S4**), reinforcing that *At*PHT1;1/2/3 are downstream effectors of *At*CNIH5. Next, we determined the Pi uptake of radioactive tracer (P^{32}) per plant using a real-time imaging system (Kanno et al., 2016). When Pi is replete, there were no significant differences in the Pi uptake within 15 minutes between WT and *cnih5*; however, the shoot-to-root distribution of P^{32} significantly altered in the *cnih5* (**Fig. 4D**). Under Pi deficiency, loss of *AtCNIH5* resulted in an 18% reduction of P^{32} uptake relative to the WT, while the shoot-to-root distribution of P^{32} was comparable between the two genotypes (**Fig. 4D**). Overall, *cnih5* showed reduced shoot Pi levels under Pi sufficiency and decreased Pi uptake under Pi deficiency, which could be ascribed to the decreased amount of *At*PHT1;1/2/3 and *At*PHT1;4, and probably other *At*PHT1s.

To answer whether *At*CNIH5 shares functional redundancy with other *At*CNIH members, we analyzed *cnih* double mutants carrying defective *AtCNIH1*, *AtCNIH3*, or *AtCNIH4* in the *cnih5* background. In the respective *cnih* double mutants, the expression of the remaining *AtCNIH* genes was not altered (**Supplementary Fig. S7**), hinting that there is no compensatory upregulation of other *AtCNIH* genes at the transcript level when *AtCNIH5* and/or other *AtCNIH* are knockout. The *cnih* double mutants did not display an exacerbated reduction of shoot Pi levels; however, the shoot and root biomass of *cnih4/5* remarkably diminished (**Supplementary Fig. S7**), indicating that simultaneous loss of *AtCNIH4* and *AtCNIH5* suppressed plant growth. When hydroponically grown under Pi-sufficient conditions, the 3-week-old *cnih4/5* plants were also smaller than the WT and *cnih5* plants; under Pi-deficient conditions, the shoot biomass of the *cnih3/5* and *cnih4/5* plants was

reduced relative to the *cnih5* (**Supplementary Fig. S8**). Unexpectedly, the Pi concentrations showed no differences between the WT and *cnih5* adult plants, while the shoot and root Pi levels in the *cnih4/5* adult plants were increased relative to the *cnih5* under Pi-deficient conditions (**Supplementary Fig. S8**). Taken together, *At*CNIH5 is the predominant *At*CNIH member functionally linked to the regulation of Pi uptake at the seedling stage. As plants grow to an older stage in hydroponics, other *At*CNIH members affect plants' fitness and also participate in maintaining Pi homeostasis.

Loss of *AtCNIH5* leads to decreased plasma membrane localization of *At*PHT1;1

To prove that *At*CNIH5 is a *bona fide* ER cargo receptor of *At*PHT1s, we sought to check the subcellular distribution of *At*PHT1;1 in *cnih5*. For equal transgene expression, a homozygous line (*At*PHT1;1-S11/GFP1–10) co-expressing *At*PHT1;1-S11 driven by the native *At*PHT1;1 promoter and GFP1–10 driven by the 35S promoter was generated in the WT background and outcrossed to the *cnih5* mutant. The F2 progeny were screened for moderate fluorescence signals and subjected to genotyping. F3 individuals prorogated from the F2 plants with either the WT (+/+) or *cnih5* (–/–) background were used for confocal imaging analysis. Under Pi sufficiency, the fluorescence signals of *At*PHT1;1-S11/GFP1–10 plants in the WT background were relatively weak. So, we focused on the subcellular localization of *At*PHT1;1-S11 in the area where *AtPHT1;1* is expressed under Pi limitation. In the WT background, *At*PHT1;1-S11 accumulated at the PM in the root epidermis of the transition/elongation zone (**Fig. 5A** and **5B**) and the root hairs of the differentiation/maturation zone (**Fig. 5C**). By contrast, *At*PHT1;1-S11 in the *cnih5* background occasionally distributed into the intracellular reticular or punctate structures in these regions (**Fig. 5B**, **5C,** and **Table 1**), and the fluorescence signals significantly declined at the PM by nearly 50% (**Fig. 5A** and **5C**). Hence, we conclude that *At*CNIH5 facilitates the ER export and thus the PM targeting of *At*PHT1;1, particularly in the elongating root epidermis and root hair.

***At*CNIH5 and *At*PHF1 act in concert to control the ER exit of *At*PHT1s**

The ER-resident *At*PHF1 was previously known to regulate the ER exit of *At*PHT1s. We

thus conjectured whether the decreased PM targeting of *At*PHT1s in *cnih5* is indirectly due to an altered expression of *At*PHF1. To our surprise, *At*PHF1 levels increased by nearly 1.3-fold in the root total proteins of *cnih5* under both Pi regimes (**Supplementary Fig. S6**), even though the transcript level of *AtPHF1* was not upregulated (**Supplementary Fig. S5**). These results implied that *At*PHF1 is upregulated likely to compensate for the loss of *At*CNIH5. Considering that *At*CNIH5 interacts with both *At*PHT1;1 and *At*PHF1, we suspected that *At*CNIH5 collaborates with *At*PHF1 to assist the ER exit of *At*PHT1s. To explore this possibility, we characterized *phf1/cnih4*, *phf1/cnih5*, and *phf1/cnih4/5* mutants. Compared to the *phf1* and *phf1/cnih4* seedlings, the shoot and root biomass of *phf1/cnih5* and *phf1/cnih4/5* mutants were further reduced (**Fig. 6A**). However, these mutants showed no differences in the shoot and root Pi levels compared to the *phf1* (**Fig. 6B**). In accordance with these results, the amount of *At*PHT1;1/2/3 in the total root proteins was comparable in these mutants (**Fig. 6C**). In contrast, at the adult-plant stage in hydroponic solutions, the *phf1/cnih4*, *phf1/cnih5*, and *phf1/cnih4/5* mutants displayed reduced shoot growth relative to the *phf1* (**Supplementary Fig. S9**). Of note, the *phf1/cnih5* and *phf1/cnih4/5* plants exhibited reduced shoot Pi levels relative to the *phf1* under Pi sufficiency (**Supplementary Fig. S9**). Therefore, the extra loss of *AtCNIH5* in the *phf1* background aggravates the growth retardation and further reduces Pi accumulation in the shoot when plants grow to an older stage.

_At_CNIH5 alleviates the Pi toxicity of _pho2_ but is not a direct target of _At_PHO2

To address whether *At*CNIH5 acts downstream of the *At*PHO2-mediated Pi homeostasis pathway, we generated the *pho2/cnih5* mutant. Compared to *pho2*, *pho2/cnih5* accumulated less Pi in the shoot to a similar extent as reported for *pho2/pht1;1* (**Fig. 7A**) (Huang et al., 2013) and exhibited reduced *At*PHT1;1/2/3 and *At*PHT1;4 relative to the *pho2* (**Fig. 7B**). By comparison, the expression level of the xylem loading Pi transporter *At*PHO1 was increased in *pho2/cnih5* (**Fig. 7B**), suggesting that defective *AtCNIH5* specifically impairs the ER export of *At*PHT1s. We next explored whether *At*PHO2 functions as a hypothesized E2/E3 hybrid enzyme to mediate the downregulation of *At*CNIH5. Using the *N. benthamiana* transient expression system, we found that in contrast to *At*PHO2-mediated degradation of *At*PHO1 in a dosage-dependent manner as previously reported (Liu et al., 2012), neither the

catalytically defective *At*PHO2^{C748A} interacted with *At*CNIH5 nor the catalytically active *At*PHO2 suppressed the expression of *At*CNIH5 (**Supplementary Fig. S10**). Taken together, although the loss of *AtCNIH5* alleviates the Pi toxicity of *pho2* as a result of downregulation of *At*PHT1s, we have no evidence to support *At*CNIH5 as a direct target of *At*PHO2.

DISCUSSION

*At*CNIH5 is a Pi starvation-induced and cell type-specific ER cargo receptor for *At*PHT1s

Our study provides multiple lines of evidence showing that *At*CNIH5 is a Pi starvation-induced ER cargo receptor that facilitates the PM targeting of *At*PHT1s. Gene expression profiles using GUS and GFP reporters and subcellular distribution analyses of fluorescent protein fusions suggest *At*CNIH5 as the sole *At*CNIH member induced by low Pi in the root outer layers (**Fig. 1A**, **1B**, **Supplementary Fig**. **S1**, and **S2**). We also showed that *At*CNIH5 localized to the ER and was closely associated with the ERES makers *At*SAR1A, *At*SEC16A, and *At*SEC24A (**Fig. 2A**–**C**). As *At*CNIH5 interacts with *At*PHT1;1/2/3, *At*PHT1;4 and *At*PHF1 (**Fig. 3A**–**C**), it is likely that *At*CNIH5 participates in the COPII-mediated ER-to-Golgi transport of *At*PHT1s. We surmise that the recognition of *At*PHT1s by *At*SEC24s alone is not an efficient signal to drive the ER exit of *At*PHT1s, and therefore requires the coincident or successive interaction of *At*PHT1s with *At*CNIH5 and *At*PHF1 (see the discussion in the next section). Although *AtCNIH5* is expressed at a lower level than *AtCNIH1*, *AtCNIH3,* and *AtCNIH4* under Pi sufficiency (**Fig. 1A**), the impairment of *AtCNIH5* diminished the amount of *At*PHT1;1–1;4 by 40–50% in the root microsomal fractions (**Fig**. **4C**). The results of confocal imaging also corroborated a lower efficiency of PM targeting and higher intracellular retention of *At*PHT1;1-S11 in the epidermis within the root transition/elongation zone and the root hair of *cnih5* (**Fig. 5** and **Table 1**). Our side-by-side proteomic analysis also identified *At*PHT1s as the prominent membrane cargoes of *At*CNIH5 under Pi starvation (Liu et al., 2024), thus reinforcing the conclusion that *At*CNIH5 mediates the ER export of *At*PHT1s and, thus, their PM targeting. Since the promoter-reporter activities of *AtCNIH1*, *AtCNIH3,* and *AtCNIH4* are barely detected in the outer layers of the primary root (**Supplementary Fig. S1**), where *AtPHT1;1–1;4* genes are mainly

expressed, we infer that *At*CNIH5 is the predominant *At*CNIH member regulating the PM trafficking of *At*PHT1s. Although the *AtCNIH4* transcript is the most abundant among the family, based on the phenotypes of *cnih4* and *cnih4/5*, *At*CNIH4 seems to play a minor role in modulating Pi homeostasis at the seedling stage. Indeed, *At*CNIH isoforms have been reported to have the potential to form tissue- or cell-type-dependent oligomers (Wudick et al., 2018), which may affect the ER export of *At*PHT1s to a varying degree. Intriguingly, belonging to the *Brassicaceae* family devoid of mycorrhizal symbiosis, *Arabidopsis* species was suggested to take advantage of rapid root growth and root hair formation as a strategy for Pi uptake when grown under Pi depletion (Lambers et al., 2008). In agreement with this notion, we observed a less apparent reduction of Pi level in the 11-day-old *cnih5* seedlings (18% reduction; **Fig. 4B**) than in the 5-day-old *cnih5* seedlings (30% reduction; **Supplementary Fig. S5**), in which macro-scale architectures of the root system were still undeveloped. In other words, our data support that the *Brassicaceae*-specific *At*CNIH5 may play a more crucial role in enhancing Pi uptake at the elongating root epidermis and root hairs at the early seedling stage.

The interplay of *At*PHF1 and *At*CNIHs in regulating the ER exit of *At*PHT1s

Our work showed that *At*PHF1 and *At*CNIH5 interact in the ER and likely cooperate to modulate the ER exit of *At*PHT1;1 in a cell type-dependent manner. The SEC12-related plant-specific PHF1 was previously proposed to functionally resemble the yeast ER-resident protein Pho86 (González et al., 2005). As the *in vitro* vesicle budding assay indicated, the yeast Pho86 may assume a conformation of Pi transporter Pho84 competent for specific incorporation into COPII vesicles or to recruit COPII proteins to the ER (Lau et al., 2000). By comparison, the yeast Erv14 cycles between the ER and the Golgi, and the ER membranes lacking functional Erv14 exhibit less efficient incorporation of cargoes into COPII vesicles (Powers and Barlowe, 2002). In accordance, the live-cell imaging results revealed a reduction of the kinetics of ER exit of Erv14's cargoes in the *erv14Δ* mutant (Herzig et al., 2012). Their findings align with our current view on the role of *At*CNIH5 in boosting the ER exit of *At*PHT1s. While split-GFP-tagged *At*PHT1;1 mainly distributed at the PM of root cells in the WT under Pi depletion, it was in part retained intracellularly in the epidermis within the root

transition/elongation zone and the root hair of *cnih5* (**Fig. 5B**, **5C** and **Table 1**). These observations suggested a less efficient PM targeting of *At*PHT1;1 without *At*CNIH5. By contrast, *At*PHT1;1-S11 in the *phf1* was barely detectable at the PM of the epidermal cells throughout the different developmental zones, including the lateral root cap (**Supplementary Fig. S11**). When enhancing the laser power, we could discern the weak *At*PHT1;1-S11-labled punctate structures that may represent the intermediates *en route* to degradation, thus in line with the severe reduction of *At*PHT1;1/2/3 in *phf1* (**Fig. 6C**). In contrast, the intracellularly retained *At*PHT1;1-S11 in the Pi-limited root of *cnih5* could be eventually subjected to degradation using routes other than the conventional endocytic pathway, as revealed by the poor co-localization of *At*PHT1;1-S11 with the FM4-64-labeled compartments upon Concanamycin A (Conc A) treatment (**Supplementary Fig. S12**).

We envisage that, unlike the unicellular yeast, higher plants have adopted a mechanism to jointly engage PHF1 and CNIHs in specific cell types to select and pack PHT1s for the COPII-mediated transport. *At*PHF1 impairs the ER exit of *At*PHT1s throughout the root (Bayle et al., 2011). By contrast, *At*CNIH5 impacts the PM trafficking of *At*PHT1s, particularly in the elongating root epidermis and root hairs (**Fig. 5A** and **5C**). As the proliferation of root hair is a crucial trait for improving Pi acquisition under Pi limitation (Gahoonia and Nielsen, 1998; Tanaka et al., 2014), it would be interesting to investigate the physiological relevance of *At*CNIH5 in modulating the PM trafficking of *At*PHT1s in root hair cells. It is also worth mentioning that we did not detect the interaction of *At*PHF1 with *At*CNIH1, *At*CNIH3, and *At*CNIH4 in the yeast split-ubiquitin system (unpublished**,** Liu et al.). This implied that even in the vascular tissues, where *AtPHF1* and *AtCNIH* genes are highly expressed, *At*PHF1 may preferentially interact with *At*CNIH5 over the other *At*CNIH isoforms. According to single-cell mRNA sequencing (scRNA-seq) analyses, *AtCNIH5* shows a trend of gradually increased expression in the root epidermis and cortex along the developmental axis (**Supplementary Fig. S13**) (Shahan et al., 2022; Trevor et al., 2022). This underscores a significant role for *At*CNIH5 in facilitating Pi uptake beyond the root apical meristem and primarily at the outer root cell layers of the non-proliferating domains.

AtPHF1 is mainly expressed in the root tip and stele under Pi sufficiency and can be further induced in the external root layers at low Pi availability (Bayle et al., 2011). This

pattern coincides with the Pi starvation-induced expression of *AtCNIH5* in the epidermis and cortex, whereas the gene activity of *AtCNIH5* is absent in the root apical meristem (**Fig. 1B** and **Supplementary Fig. S2**). Although the compensation mechanism underlying the upregulation of *At*PHF1 in *cnih5* remains obscure (**Supplementary Fig. S6**), the additional loss of *AtCNIH5* in the *phf1* did not synergistically reduce cellular Pi levels but severed plant growth (**Fig. 6B**). This led to the idea that *At*PHF1 and *At*CNIH5 may not play a functionally redundant role but have epistatic relationships concerning their role in the ER exit of *At*PHT1s. Future analysis of *At*CNIH5 overexpressors in the *phf1* background can help answer whether *At*CNIH5 can replace or bypass *At*PHF1 functionally. We cannot exclude the possibility that the lack of these two components further suppressed the plant growth due to exaggerated cytoplasmic Pi inadequacy. Alternatively, but not mutually exclusive to this scenario, *At*CNIH5 may have some downstream effectors other than *At*PHT1s that exacerbate the growth retardation of *phf1/cnih5*. Based on our present study, we propose a hypothetical working model as to how *At*PHF1 and *At*CNIH5 interplay to assist the ER exit of *At*PHT1s (**Fig. 8**). *At*PHF1 interacts with *At*PHT1s at the ER to ensure their competence for the ER exit, accompanied by the COPII assembly at the ERES of nearly every cell type in the root. On the other hand, *At*CNIH5 acts at a later step, perhaps by selectively loading *At*PHT1s at ERES into the COPII-mediated trafficking pathway in the non-dividing root cells, including the epidermis within the transition/elongation zone and the elongating root hair of the differentiation zone. More studies are needed to define the interaction of *At*PHT1s, *At*PHF1, and *At*CNIH5 in a time and space manner.

Materials and methods

Plant material and growth conditions

All *A. thaliana* plants used in this study were in Columbia-0 (Col-0) ecotype. Seeds of wild-type (WT), *cnih4* (SALK_145991), *cnih5* (SAIL_256_B03), *phf1* (SALK_037068), and *pho2-1* (Delhaize and Randall, 1995) were obtained from the Arabidopsis Biological Resource Center (ABRC). The *cnih1/5* (SAIL_117_E12 for *cnih1* and SAIL_256_B03 for *cnih5*) and *cnih3/5* (GABI_300F09 for *cnih3* and SAIL_256_B03 for *cnih5*) mutants were previously characterized as described (Wudick et al., 2018). *A. thaliana* seeds were surface-

sterilized, germinated, and grown on plates with modified one-half strength Hoagland nutrient solution containing 250 μM KH_2PO_4, 1% sucrose, and 0.8 or 1.2% Bacto agar (BD Difco™ 214010) in the growth chamber at 22 °C with a 16-h light/8-h dark cycle. The Pi-sufficient (+P) and Pi-deficient (−P) media were one-half strength Hoagland nutrient solutions containing 250 μM and without KH_2PO_4, respectively. The N-deficient (−N) media were one-half strength Hoagland nutrient solutions containing either 0 μM or 0.1 mM KNO_3. For hydroponic growth of *A. thaliana* adult plants, 1–2-week-old seedlings were transferred to +P one-half strength Hoagland solutions without a supplement of sucrose and grown for additional days in +P or −P media as indicated in figure legends. For *N. benthamiana* plants, seeds were surface-sterilized and germinated on half-strength Murashige and Skoog (MS) medium. Three to four-week-old plants were used for *Agrobacterium* infiltration for transient overexpression.

Genomic DNA extraction and genotyping of mutants

Genomic DNA was extracted from the leaves of 2-week-old plants with the extraction buffer containing 200 mM Tris-HCl (pH 7.5), 250 mM NaCl, 25 mM EDTA (pH 8.0) and 0.5% SDS. Polymerase chain reaction (PCR) was then performed to validate the presence of the T-DNA alleles of *phf1*, *cnih4*, *cnih5*, or the *pho2* point mutation in samples as previously described (Delhaize and Randall, 1995). Primer sequences used are listed in **Supplementary Table S1**.

RNA isolation, reverse transcription PCR (RT-PCR) and quantitative RT-PCR (RT-qPCR)

Total root RNA was isolated using GENEzol™ TriRNA Pure Kit with DNase (GZXD200, Geneaid), and a 500-ng RNA was used for the first-strand cDNA synthesis using PrimeScript™ 1st strand cDNA Synthesis Kit (6110A, TaKaRa) with oligo(dT) primer. RT-qPCR was performed using KAPA SYBR® FAST qPCR Master Mix (2×) Kit on StepOnePlus™ Real-Time PCR System (Applied Biosystems) according to the manufacturer's instructions. Gene expression values were normalized to the internal reference *ACT8* (AT1G49240). Transcript expression levels of *AtCNIH* genes in WT, *cnih*

single, and *cnih* double mutants were examined by either RT-PCR or RT-qPCR. Primer sequences used are listed in **Supplementary Table S1**.

Construct design and yeast split-ubiquitin assay

For constructing the yeast expression clones, the coding sequence (CDS) of *AtCNIH5* and *AtPHT1;4* was amplified by PCR, cloned into the pCR8/GW/TOPO vectors and sequenced. The pCR8/GW/TOPO constructs containing the CDS of *AtPHT1;1* and *AtPHF1* were cloned as previously reported (Huang et al., 2013). The CDS of *AtCNIH5* was recombined into the commercially synthesized MET17-PLV-Cub_GW through an LR reaction, resulting in the N-terminally fused PLVCub-*At*CNIH5. The CDS of *AtPHF1*, *AtPHT1;1*, and *AtPHT1;4* was recombined into NX32_GW (ABRC plasmid CD3-1737; Obrdlik et al., 2004) through LR reactions, resulting in C-terminally fused Nub fragments (NubG-*At*PHF1 and NubG-*At*PHT1;1). The Nub and Cub expression clones were sequentially transformed into the yeast THY.AP4 strain (ABRC CD3-808; Obrdlik et al., 2004). Fresh yeast colonies picked from Yeast Extract Peptone Dextrose Adenine (YPDA) medium or Synthetic Complete (SC) medium without leucine (SC–L) were inoculated in corresponding liquid medium and incubated overnight at 30 °C with shaking at 200 rpm. Overnight yeast culture was then diluted to OD_{600} = 0.2 and grew for another 5 to 12 h until OD_{600} reached 0.8. Yeast pellet was collected by centrifugation at 2,000×g at 4 °C for 5 min, washed with ddH_2O, and resuspended in Tris-EDTA/lithium acetate solution (TE/LiAc, 10 mM Tris-HCl [pH 8.0], 1 mM EDTA, and 0.1 M lithium acetate). The PLVCub-*At*CNIH5-containining transformants were selected and maintained on SC–L for sequential transformation with NubWT (positive control), NubG (negative control), NubG-*At*PHT1;1 or NubG-*At*PHF1. Yeast transformants with Nub- and PLV-Cub fusions were selected and maintained on SC medium without leucine and tryptophan (SC–LW). For the protein-protein interaction testing, yeast cells co-expressing PLVCub-*At*CNIH5 and NubG-*At*PHT1;1, NubG-*At*PHT1;4, or NubG-*At*PHF1 were plated on synthetic media lacking leucine, tryptophan, adenine, and histidine (SC–LWAH) with 500 μM methionine or on SC–LW containing 2 g/L 5-bromo-4-chloro-3-indolyl-β-d-galactopyranoside (X-Gal). Primer sequences used are listed in **Supplementary Table S2**.

Construct design for subcellular localization analysis in *N. benthamiana* leaves

For constructing the *UBQ10*:*sXVE*: S10-*At*CNIH5 and *UBQ10*:*sXVE*: mCherry-*At*CNIH5 clones, the CDS of *AtCNIH5* was amplified by PCR and subcloned into *UBQ10*:*sXVE*: S10-(MCS) (Addgene plasmid # 108177; Liu et al., 2018; Liu, 2021) using AscI/XhoI and AscI/BamHI sites, respectively. For constructing the *UBQ10*: *At*SEC16A-S11 clones, the CDS of *AtSEC16A* was amplified by PCR and subcloned into *UBQ10:* (MCS)-S11 using AscI/SalI sites. The plasmid encoding *35S*: RFP-*At*CNIH5 was described as previously reported (Wudick et al., 2018). The plasmid encoding *35S*: ER-mCherry (CD3-959; Nelson et al., 2007) was obtained from ABRC. Primer sequences used are listed in **Supplementary Table S2**.

Construct design for the tripartite split-GFP assay in *N. benthamiana* leaves

For constructing the *UBQ10*:*sXVE*: S10-*At*PHF1 and *UBQ10*:*sXVE*: S10-*At*PHO1 clones, the CDS of *AtPHF1* and *AtPHO1* were amplified by PCR and subcloned into *UBQ10*:*sXVE*: S10-(MCS) (Addgene plasmid # 108177; Liu et al., 2018; Liu, 2021) using AscI/PacI sites. For constructing the *UBQ10*:*sXVE*: *At*PHT1;1-S11 and *UBQ10*:*sXVE*: *At*PHO2^{C748A}-S11 clones, the CDS of *AtPHT1;1* and *AtPHO2* ^{C748A} were amplified by PCR and subcloned into *UBQ10*:*sXVE*: (MCS)-S11 (Addgene plasmid # 108179; Liu et al., 2018; Liu, 2021) using XbaI/SpeI and AscI/SpeI sites, respectively. For the tripartite split-GFP reconstitution, the constructs encoding S10-tagged and S11-tagged protein fusions were co-expressed in the presence of *UBQ10*:*sXVE*: GFP1–9 (Addgene plasmid # 108187; Liu et al., 2018; Liu, 2021). Co-expression with S10-3xHA or 3xHA-S11 was used as a negative control for protein–protein interaction. Primer sequences used are listed in **Supplementary Table S2**.

Construct design and protein degradation assay in *N. benthamiana* leaves

For constructing *UBQ10*:*sXVE*: S10-*At*PHO2 clone, the CDS of *AtPHO2* were amplified and subcloned into pGPTVII using AscI/SpeI and AscI/XbaI sites. *A. tumefaciens* carrying *UBQ10*:*sXVE*: S10-*At*PHO2, *UBQ10*:*sXVE*: S10-*At*CNIH5 and *UBQ10*:*sXVE*: S10-*At*PHO1 were infiltrated into tobacco leaves, each with a final OD_{600} in the range of 0.01–0.05. *A.*

tumefaciens carrying *UBQ10*:*sXVE*: GFP (Schlücking et al., 2013) was co-infiltrated at a final OD_{600} of 0.01 as an internal control.

Agrobacterium tumefaciens-mediated infiltration of _N. benthamiana_ leaves

Agrobacterium tumefaciens strain EHA105 harboring the expression constructs or p19 was incubated in Luria–Bertani (LB) medium with the appropriate antibiotics [gentamicin (50 μg ml^{-1}), rifampicin (5 μg ml^{-1}) or kanamycin (50 μg ml^{-1})]. Cells were resuspended in the infiltration medium containing 10 mM $MgCl_2$, 10 mM MES (pH 7.5), and 150 μM acetosyringone, and co-infiltrated to the true leaves of 3–4-week-old tobacco plants. For the inducible gene expression, 36.7 μM β-estradiol was applied as previously described (Liu et al., 2018; Liu, 2021). The infiltrated leaves were collected 2 days post-infiltration (dpi) for confocal imaging or protein extraction.

Construct design and the generation of _Arabidopsis_ transgenic plants

The CDS of a gene was amplified by PCR, cloned into the pJET1.2/blunt cloning vector, and sequenced before subcloning into the desired expression vectors. For constructing the *AtCNIH1/3/4/5pro:* GUS and *AtCNIH5pro:* GFP reporter clones, the genomic sequence containing the promoter region of *AtCNIH1* (−497 to +134; transcription start site designated as +1), *AtCNIH3* (−1,793 to +225), *AtCNIH4*, (−1,717 to +303), and *AtCNIH5* (−1,701 to +304) was each amplified by PCR and subcloned into pMDC163 or pMDC111 using PacI/AscI sites.

For constructing the *AtCNIH5* genomic clone (*AtCNIH5pro*: *AtCNIH5*) to complement *cnih5*, the genomic sequence *AtCNIH5*, including the putative promoter region with 5′ UTR (−1,963 to +304) and the genomic sequence containing 3′ UTR (+305 to +1,324) were amplified, and cloned into pMDC32 using In-Fusion HD cloning (TaKaRa) for sequencing. Based on the *AtCNIH5* genomic construct clone, the genomic GFP-*AtCNIH5* construct (*AtCNIH5pro*: GFP-*AtCNIH5*) was generated by inserting GFP at the N-terminus of *AtCNIH5* using In-Fusion HD cloning and transformed into the *Arabidopsis cnih5* plants. For the generation of *35S*: RFP-*At*CNIH5 transgenic lines, the construct was generated in the backbone of pH7WGR2 through an LR reaction as previously described (Wudick et al.,

2018).

For the subcellular localization analysis of *At*PHT1;1-S11 in *AtPHT1;1pro*: *At*PHT1;1-S11/*35S*: GFP1–10 transgenic plants, a homozygous line expressing *35S*: GFP1–10 was first established and then transformed with the *AtPHT1;1pro*: *At*PHT1;1-S11 construct. For constructing of *35S*: GFP1–10, the CDS of GFP1–10 was amplified and subcloned into pMDC201 using SpeI/EcoRI sites. For constructing *AtPHT1;1pro*: *At*PHT1;1-S11, the putative *AtPHT1;1* promoter region (−1,964 to +494) and the CDS of *At*PHT1;1 was subcloned into pGPTVII binary vector using NotI sites. All primer sequences used for gene cloning in this study are listed in **Supplementary Table S2**.

Agrobacterium tumefaciens-mediated _Arabidopsis_ transformation

Binary expression vectors were transformed into *Agrobacterium tumefaciens* strain GV3101 (pMP90) and then transformed into *Arabidopsis* by floral dip method (Clough and Bent, 1998). T2 transgenic lines with a segregation ratio of 3 resistant: 1 sensitive were selected for T3 propagation. Only T3 homozygous lines were used for further analyses.

Confocal microscopy

Confocal microscopy images were acquired using Zeiss LSM 800 (Zeiss) with objectives Plan-Apochromat 10×/0.45 M27, 20×/0.8 M27, and 40×/1.3 Oil DIC M27 in multi-track mode with line switching and averaging of two reading. Excitation/emission wavelengths were 488 nm/410−546 nm for GFP, 561 nm/560−617 nm for RFP and mCherry, and 488 nm/571−700 nm for FM4-64. For subcellular localization analysis of *At*PHT1;1-S11, the seedings were kept in dark for 4 h prior to the experiments.

Histochemical staining of β-glucuronidase (GUS analysis)

GUS staining were performed as previously described (Li, 2011). Seedlings were submerged in freshly prepared X-Gluc staining buffer containing 500 mM NaH_2PO_4, 500 mM $Na_2HPO_4 \cdot 7H_2O$, 1mM $K_3Fe(CN)_6$, 1 mM $K_4Fe(CN)_6$, 10 mM EDTA, 0.1% Triton X-100, and 2.25 mM X-glucuronide (Cyrusbioscience), vacuumed for 20 min, and then incubated at 37 °C for 2 to 2.5 h. The pigments were serially washed out at each step through

10% to 99% ethanol for 30 min. Finally, the GUS staining was examined under a stereo microscope (ST3E-0745) and Leica DM2500 microscope (Leica).

Pi concentration and Pi uptake analysis

Pi concentrations were analyzed as described (Ames, 1966) with minor modifications. For the extraction of Pi, fresh tissue was homogenized with 1% glacial acetic acid and incubated at 42 ℃ for 30 min followed by centrifugation at 13,000×g for 5 min to obtain clear supernatant. For the measurement of Pi concentration, the supernatant aliquot was mixed with the assay solution (0.35% NH_4MoO_4, 0.86 N H_2SO_4 and 1.4% ascorbic acid) and incubated at 42 ℃ for 30 min. Pi concentrations were measured at A_{750}. Pi uptake in the whole seedling was measured in +P or −P medium supplemented with ^{32}P as previously described (Kanno et al., 2016).

Total protein, microsomal protein, plasma membrane-enriched protein extraction

For the extraction of total proteins, the tobacco leaves and *Arabidopsis* roots were ground in liquid N and dissolved in protein lysis buffer containing 60 mM 2-amino-2-(hydroxymethyl)-1,3-propanediol-HCl (pH 8.5), 2% SDS, 2.5% glycerol, 0.13 mM EDTA, 1 mM phenylmethylsulfonyl fluoride and Protease Inhibitor Cocktail (P9599; Sigma-Aldrich). *Arabidopsis* root microsomal proteins were extracted using Minute™ Plant Microsomal Membrane Extraction Kit (MM-018, Invent Biotechnologies), and resuspended in the same protein lysis buffer used for total protein extraction.

Immunoblot analysis

For *Arabidopsis* seedlings, a total of 25 μg root total proteins and 15 μg root microsomal proteins from each sample were loaded onto 4–12% Q-PAGE™ Bis-Tris Precast Gel (SMOBIO) or NuPAGE 4–12% Bis-Tris Gels (Thermo Fisher Scientific). For tobacco leaves, a total of 25 μg leaf total proteins from each sample were loaded onto gels. Gel was transferred to polyvinylidene difluoride membranes (IPVH00010 Immobilon-P Membrane, Merck). Membrane was blocked with 1 or 2% BSA in 1× PBS solution with 0.2% Tween 20 (PBST, pH 7.2) at RT for 1 h, and washed 4 times with 1× PBST for 5 min followed by

hybridization with primary antibodies of *At*PHT1;1/2/3 (1:1,000, PHY0753, PhytoAB), *At*PHT1;4 (Huang et al., 2013), GFP (1:5,000, AS214696, Agrisera) and S10 (1:1,000) for overnight at 4 °C; *At*PHF1 (Huang et al., 2013) and *At*PHO1 (Liu et al., 2012) at RT for 2 h in blocking solution. Anti-S10 polyclonal rabbit antibody was raised against the peptide of S10 (MDLPDDHYLSTQTILSKDLN) (Liu et al., 2018) and produced by LTK BioLaboratories, Taiwan. The membrane was washed four times with 1× PBST for 5 min followed by hybridization with the horseradish peroxidase–conjugated secondary antibody (1:20,000, GTX213110-01 and 1:10,000, GTX213111-01, GeneTex) in blocking solution at RT for 1 h. After four washes in 1× PBST for 5 min and a rinse with distilled water, chemiluminescent substrates (WesternBright ECL and WesternBright Sirius ECL, Advansta) were applied for signal detection.

Co-immunoprecipitation

The root of *Arabidopsis* 11-day-old *UBQ10*: GFP and *AtCNIH5pro*: GFP-*AtCNIH5/cnih5* complementation (COM) seedlings were grown under Pi-deficient (–P, 0 μM KH_2PO_4, seven days of starvation) conditions and ground in liquid N. Root membrane fraction was isolated by the low-speed pellet (LSP) method as previously described (Yoshimoto et al., 2004) and dissolved in protein lysis buffer containing 100 mM Tris-HCl (pH 7.5), 400 mM sucrose, 1 mM EDTA, 1% Triton X-100, 1 mM phenylmethylsulfonyl fluoride and Protease Inhibitor Cocktail (P9599; Sigma-Aldrich). The equivalent of 30 μg root membrane-enriched protein was loaded onto 5 μl of GFP-Trap beads (gta-10; Chromotek) and incubated at 4 °C for 2 h. After binding, the agarose beads were washed once with the protein lysis buffer mentioned above without Triton X-100 and resuspended in 1× Laemmli buffer, followed by boiling at 95 °C for 5 min. The supernatant was collected for immunoblot analysis.

Root growth analysis

For the measurement of primary and lateral root lengths, photos of roots were taken by a PowerShot G16 Camera (Canon), and the length was measured using ImageJ segmented line function (Schneider et al., 2012). Only lateral roots with lengths longer than 2 mm were included for measurement. For the measurement of root hair length, seedlings were grown

on Pi-sufficient (+P) and Pi-deficient (−P) media containing 0.6% Bacto agar. Root hairs were observed under the Leica DM2500 microscope equipped with DIC optics and photographed. The ten longest root hairs within the maturation zone per root, as defined from 5 mm to 10 mm away from the root tip, were measured by ImageJ. Root hair numbers within the above-mentioned maturation zone were counted for root hair density.

Chemical treatments

Acetosyringone (150 mM stock in DMSO; D134406; Sigma-Aldrich) was diluted to a final concentration of 150 μM in ddH_2O. β-estradiol (36.7 mM stock in ethanol; E2758; Sigma-Aldrich) was diluted to a final concentration of 36.7 μM in ddH_2O. Conc A (1 mM, cat. 11050, Cayman) was diluted to a final concentration of 1 μM in DMSO. FM4-64 (4 mM stock in DMSO; T3166; Invitrogen) was diluted to a final concentration of 4 μM in an appropriate medium.

Accession Numbers

Sequence data from this article can be found in the Arabidopsis Genome Initiative under the following accession numbers: *At*CNIH1 (AT3G12180), *At*CNIH3 (AT1G62880), *At*CNIH4 (AT1G12390), *At*CNIH5 (AT4G12090), *At*PHT1;1 (AT5G43350), *At*PHT1;4 (AT2G38940), *At*PHF1 (AT3G52190), *At*PHO1 (AT3G23430), *At*PHO2 (AT2G33770), *At*SEC16A (AT5G47480), *At*SEC24A (AT3G07100), and *At*SAR1A (AT2G33120).

SUPPLEMENTARY DATA

The following materials are available in the online version of this article.

Supplementary Figure S1. Expression of *AtCNIH1pro:* GUS, *AtCNIH3pro:* GUS and *AtCNIH4pro:* GUS in *Arabidopsis*.

Expression of *AtCNIH1pro*: GUS, *AtCNIH3pro*: GUS, and *AtCNIH4pro*: GUS in the primary (A) and lateral roots (B) of 7-day-old *Arabidopsis* seedlings grown under Pi-sufficient (+P, 250 μM KH_2PO_4) and Pi-deficient conditions (–P, 0 μM KH_2PO_4, five days of starvation). Scale bars, 100 μm.

Supplementary Figure S2. Expression of *AtCNIH5pro:* GFP in *Arabidopsis*.

Expression of *AtCNIH5pro*: GFP in 5-day-old *Arabidopsis* seedlings grown under Pi-sufficient (+P, 250 μM KH_2PO_4) and Pi-deficient (–P, 0 μM KH_2PO_4, five days of starvation) conditions. The primary root's maturation zone, basal meristem, and apical meristem are shown as indicated. Merged images of green fluorescence and bright field channels are shown. Scale bars, 50 μm.

Supplementary Figure S3. Expression of *35S*: RFP-*At*CNIH5 in *Arabidopsis*.

Expression of *35S*: RFP-*At*CNIH5 in 5-day-old *Arabidopsis* seedlings grown under Pi-deficient (–P, 0 μM KH_2PO_4, five days of starvation) conditions. Scale bars, 50 μm.

Supplementary Figure S4. Complementation of *cnih5* by the expression of the genomic *AtCNIH5* and GFP-*AtCNIH5* sequences.

(A) The shoot fresh weight (FW) and Pi level of 11-day-old seedlings of *Arabidopsis* WT, *cnih5*, and *AtCNIH5pro*: *AtCNIH5/cnih5* complementation (COM) lines grown under Pi-sufficient (+P, 250 μM KH_2PO_4) conditions. Error bar represents SE (n = 9, pools of seedings from independent experiments; WT or complemented plants versus *cnih5*, $^*P < 0.05$, $^*P < 0.01$; Student's t-test, two-tailed).

(B) The shoot fresh weight (FW) and Pi levels of 11-day-old seedlings of *Arabidopsis* WT, *cnih5*, and *AtCNIH5pro*: GFP-*AtCNIH5/cnih5* complementation (COM) lines grown under Pi-sufficient (+P, 250 μM KH_2PO_4) conditions. Error bar represents SE (n = 6, pools of seedings from independent experiments; complemented plants versus *cnih5*, $^*P < 0.05$, $^*P < 0.01$; Student's t-test, two-tailed).

(C) Protein expression of *At*PHT1;1/2/3 in the low-speed pellet (LSP) of *Arabidopsis* WT, *cnih5* and COM lines under Pi-deficient (–P, 0 μM KH_2PO_4, three days of starvation) conditions. The relative expression level of *At*PHT1;1/2/3 was normalized with the corresponding amido black staining and relative to the WT control. One representative immunoblot from two independent experiments is shown. Root microsomal protein was isolated by the LSP method as previously described (Yoshimoto et al., 2004).

Supplementary Figure S5. The expression of Pi starvation-induced genes and the root phenotypes of *Arabidopsis cnih5.*

(A) The transcript expression of *AtPHT1;1–1;3*, *AtACP5*, and *AtPHF1* in the root of 11-day-old *Arabidopsis* WT and *cnih5* seedlings grown under Pi-sufficient (+P, 250 μM KH_2PO_4) and Pi-deficient (–P, 0 μM KH_2PO_4, three days of starvation) conditions assessed by RT-qPCR. Error bars represent SE (n = 2, pools of seedings from independent experiments).

(B and C) The primary root (PR) length (B) and the lateral root (LR) density (C) of 9-day-old *Arabidopsis* WT and *cnih5* seedlings grown under Pi-sufficient (+P, 250 μM KH_2PO_4) and Pi-deficient (–P, 0 μM KH_2PO_4, five days of starvation) conditions. Error bar represent SE (n = 6–10 for the primary root length; n = 9 for the lateral root density; $^{*}P < 0.05$, $^{**}P < 0.01$; Student's t-test, two-tailed).

(D–F) The shoot Pi level (D), the root hair (RH) length (E) and density (F) of 5-day-old *Arabidopsis* WT and *cnih5* seedlings grown under Pi-sufficient (+P, 250 μM KH_2PO_4) or Pi-deficient (–P, 0 μM KH_2PO_4, five days of starvation in D, and three days of starvation in E and F) conditions. Error bar represents SE (shoot Pi level, n = 3, pools of seedlings from independent experiments; root hair length, n = 80–90; root hair density, n = 8–9; $^{*}P < 0.05$, $^{**}P < 0.01$; Student's t-test, two-tailed).

Supplementary Figure S6. Decreased *At*PHT1s and increased *At*PHF1 in the total root proteins from *Arabidopsis cnih5*.

Protein expression of *At*PHT1;1/2/3, *At*PHT1;4 and *At*PHF1 in the root of 11-day-old seedlings of *Arabidopsis* WT, *cnih4,* and *cnih5* under Pi-sufficient (+P, 250 μM KH_2PO_4) and Pi-deficient (–P, 0 μM KH_2PO_4, three days of starvation) conditions. The relative expression level of *At*PHT1;1/2/3, *At*PHT1;4, and *At*PHF1 was normalized with the corresponding actin and relative to the WT control. Error bars represent SE (n = 3–4, pools of seedlings from independent experiments; $^{*}P < 0.05$, $^{**}P < 0.01$; Student's t-test, two-tailed).

Supplementary Figure S7. Analyses of *Arabidopsis cnih1/5, cnih3/5*, and *cnih4/5*

seedlings.

(A) The transcript expression of *AtCNIH* genes in the root of 11-day-old *Arabidopsis* WT, *cnih5*, *cnih1/5*, *cnih3/5*, and *cnih4/5* seedlings grown under Pi-sufficient (+P, 250 μM KH_2PO_4) conditions assessed by RT-qPCR or RT-PCR.

(B and C) The shoot and root FW (B) and Pi levels (C) of 11-day-old *Arabidopsis cnih5*, *cnih1/5*, *cnih3/5*, and *cnih4/5* seedlings grown under Pi-sufficient (+P, 250 μM KH_2PO_4) and Pi-deficient (–P, 0 μM KH_2PO_4, three days of starvation) conditions. Error bars represent SE (n = 7–9, pools of seedlings from independent experiments; $^{*}P < 0.05$, $^{**}P < 0.01$; Student's t-test, two-tailed).

Supplementary Figure S8. Phenotypes of *Arabidopsis cnih5, cnih1/5, cnih3/5*, and *cnih4/5* adult plants.

The shoot and root FW (A) and Pi levels (B) of 20-day-old *Arabidopsis* WT, *cnih5*, *cnih1/5*, *cnih3/5*, and *cnih4/5* plants under Pi-sufficient (+P, 250 μM KH_2PO_4) and Pi-deficient (–P, 0 μM KH_2PO_4, five days of starvation) hydroponic conditions. Data are visualized using BoxPlotR (Spitzer et al., 2014). Center lines show the medians; the central plus signs (+) show the means; box limits indicate the 25th and 75th percentiles; whiskers extend to the 5th and 95th percentiles, and data points are plotted as dots. Data significantly different from the other groups are indicated by different lowercase letters (n = 15–18, biological replicates from independent experiments; One-Way ANOVA, Duncan's test).

Supplementary Figure S9. Phenotypes of *Arabidopsis phf1, phf1/cnih4, phf1/cnih5*, and *phf1/cnih4/5* adult plants.

The shoot and root FW (A) and Pi levels (B) of 20-day-old *Arabidopsis* WT, *phf1*, *phf1/cnih*4, *phf1/cnih5*, and *phf1/cnih4/5* plants grown under Pi-sufficient (+P, 250 μM KH_2PO_4) and Pi-deficient (–P, 10 μM KH_2PO_4, five days of starvation) hydroponic conditions. Data are visualized using BoxPlotR (Spitzer et al., 2014). Center lines show the medians; the central plus signs (+) show the means; box limits indicate the 25th and 75th percentiles; whiskers extend to the 5th and 95th percentiles, and data points are plotted as dots. Data significantly different from the other groups are indicated by different lowercase

letters (n = 15–24, biological replicates from independent experiments; One-Way ANOVA, Duncan's test).

Supplementary Figure S10. *At*PHO2 does not mediate the degradation of *At*CNIH5.
(A) Co-expression of S10-*At*CNIH5 with the catalytically defective *At*PHO2^{C748A}-S11 in the presence of GFP1–9 in *N. benthamiana* leaves. Scale bars, 20 µm. The co-expression of S10-*At*CNIH5 with *At*PHT1;1-S11 and S10-3xHA-S11 are, respectively, used as positive and negative protein–protein interaction controls.
(B) Immunoblot analysis of S10-*At*CNIH5 and S10-*At*PHO1 in *N. benthamiana* leaves under co-expression of increasing levels of S10-*At*PHO2. The co-expression of GFP was used as a negative control. Anti-S10 antibodies also detect free GFP.

Supplementary Figure S11. Impaired plasma membrane targeting of *At*PHT1;1-S11 in *Arabidopsis phf1*.
Representative images of localization of *At*PHT1;1-S11 in 5-day-old *AtPHT1;1pro*: *At*PHT1;1-S11/*35S*: GFP1–10 seedlings grown under Pi-deficient (−P, 0 µM KH_2PO_4) conditions. Independent lines in the *phf1* (A) and *cnih5* (B) backgrounds and the corresponding WT controls were used for comparison. GFP signals surrounding the nuclear membrane are indicated by arrows. RAM, Root apical meristem; TZ, transition zone; EZ, elongation zone; DZ, differentiation zone. Scale bar, 20µm.

Supplementary Figure S12. The localization of *At*PHT1;1-S11 in the Pi-limited root cells of *Arabidopsis* WT and *cnih5* upon Conc A treatment.
Representative images of localization of *At*PHT1;1-S11 in the root transition/elongation zone of *AtPHT1;1pro*: *At*PHT1;1-S11/*35S*: GFP1–10 5-day-old WT and *cnih5* seedlings grown under Pi-deficient (−P, 0 µM KH_2PO_4, five days of starvation) conditions in the presence DMSO or Conc A (1 µM, 4 h). The fluorescent lipophilic styryl dye FM4-64 (4 µM, 3h) was used for localization of endosomal compartments. Scale bars, 10 µm.

Supplementary Figure S13. Expression of *AtPHT1;1*, *AtPHT1;4*, *AtCNIH5,* and

***AtPHF1* revealed by single-cell mRNA sequencing (scRNA-seq) of *Arabidopsis* root.**

The dot plot used to visualize single-cell gene expression of *Arabidopsis* root is retrieved from ARVEX (https://shiny.mdc-berlin.de/ARVEX/), which hosts processed scRNA-seq data of wild-type samples from Shahan and Hsu et al. 2022 (Shahan et al., 2022). PctExp: Percentage of cells expressing the gene in a specific time zone and cell type; circle size represents the proportion (%) of cells expressing a given gene. AvgExp: Averaged normalized gene expression value in a specific time zone and cell type; the color of the scale bar represents the mean expression (natural log +1 pseudocount).

Supplementary Table S1. Oligonucleotides used for PCR genotyping, RT-PCR, and RT-qPCR analyses.

Supplementary Table S2. Oligonucleotides used for plasmid constructs.

ACKNOWLEDGMENTS

This work is supported by the Ministry of Science and Technology (MOST 108-2311-B-007-003-MY3) and the National Science and Technology Council (NSTC 112-2313-B-007-001-MY3). We thank Prof. José A. Feijó at the University of Maryland, USA, for sharing the *Arabidopsis cnih1/5* and *cnih3/5* mutants and plasmid encoding *35S*: RFP-*At*CNIH5. We thank Dr. Tzyy-Jen Chiou at Academia Sinica, Taiwan (R.O.C.), for sharing the *Arabidopsis phf1* mutants and anti-PHT1;4 and anti-PHF1 antibodies. We thank Dr. Liwen Jiang at the Chinese University of Hong Kong, People's Republic of China, for sharing the *Arabidopsis UBQ10*: GFP line. We acknowledge Ms. Wen-Chun Chou for constructing the plasmid encoding *35S*: GFP1–10, and Mr. Po-Ruey Huang for cloning the NubG-*At*PHT1;4 construct. We acknowledge Mr. Hong-Po Chen and Ms. Hui-Ying Chen for the genotyping of *phf1/cnih* mutants and of *AtPHT1;1pro*: *At*PHT1;1-S11/*35S*: GFP1–10 in the WT and *cnih5* backgrounds and the technical support from the confocal imaging core, National Tsing Hua University (sponsored by MOST 108-2731-M-007-001 and MOST 110-2731-M-007-001). We are grateful to and Dr. Laurent Nussaume at CEA Cadarache, France, and Dr. Tzyy-Jen Chiou for valuable comments on the manuscript.

AUTHOR CONTRIBUTIONS

T.-Y. L. conceived the project, designed, performed and analyzed the experiments. C.-Y. C., C.-D. T., J.-Y. W., M.-H. T., A. J. M., S. K., V. K. and H.-F. L. performed and analyzed the experiments. T.-Y. L. and C.-Y. C. wrote the article.

FIGURE LEGENDS

Figure 1. Pi starvation-induced expression pattern of *At*CNIH5.

(A) RT-qPCR analysis of *A. thaliana CNIH1, CNIH3, CNIH4,* and *CNIH5* in the shoot and root of 11-day-old seedlings grown under full nutrient (+P+N, 250 μM KH_2PO_4 and 7.5 mM KNO_3), Pi-deficient (–P+N, 0 μM KH_2PO_4 and 7.5 mM KNO_3, three days of starvation) and N-deficient (+P–N, 250 μM KH_2PO_4 and 0 μM KNO_3, three days of starvation) conditions. The magnified inset on the right top shows low Pi induction of *AtCNIH5* in the shoot. Error bars represent SE (n = 3, pools of seedings from independent experiments).

(B) Expression of *AtCNIH5pro*: GUS in 7-day-old seedlings grown under Pi-sufficient (+P, 250 μM KH_2PO_4) and Pi-deficient (–P, 0 μM KH_2PO_4, five days of starvation) conditions. a–f (+P; shoot part; trichome; primary root tip; primary root maturation zone; lateral root tip; lateral root maturation zone). g–j (–P; root tip; primary root maturation zone; lateral root tip; lateral root maturation zone). Scale bars, 10 mm in a, 0.1 mm in b, and 100 μm in c–j.

Figure 2. Subcellular localization of *At*CNIH5 to the ER and ERES.

(A) The ER and ERES localizations of S10-*At*CNIH5 in agro-infiltrated *N. benthamiana* leaves. mCherry-HDEL, luminal ER marker; *At*SEC16A-S11, ERES marker. Scale bars, 10 μm.

(B and C) Statistical line profile analysis of fluorescence intensity for localization of *At*CNIH5 with the ERES and *cis*-Golgi markers. Representative images and line profile analysis for RFP-*At*CNIH5 (B) and mCherry-*At*CNIH5 (C) (magenta) with the *cis*-Golgi marker MNS1-eGFP and the ERES markers *At*SAR1A-GFP, GFP-*At*SEC16A, and GFP-*At*SEC24A (green). Line profile applied and line profile output are shown. Peak distance analysis graphs showing the co-localization analysis with RFP-*At*CNIH5 and mCherry-*At*CNIH5 with the ERES and *cis*-Golgi markers. Scale bars = 1 μm. Significance was

analyzed by Kruskal–Wallis ($^{***}P < 0.001$). Error bars represent SE (n = 4 biological replicas, with at least 18 technical repeats).

(D) Localization of GFP-*AtCNIH5* in the root of *Arabidopsis* 5-day-old seedlings grown under Pi-deficient (–P, 0 μM KH_2PO_4, five days of starvation) conditions. TZ/EZ, transition zone/elongation zone; RH, root hair. Scale bars, 10 μm.

Figure 3. *AtC*NIH5 interacts with *At*PHT1;1, *At*PHT1;4, and *At*PHF1.

(A) Expression of S10-*At*CNIH5, S10-*At*PHF1, S10-3xHA and *At*PHT1;1-S11 in the presence of S11-GFP1–9 or GFP1–9 in *N. benthamiana* leaves. The co-expression of *At*PHT1;1-S11 with S10-*At*PHF1 and S10-3xHA are used as positive and negative protein–protein interaction controls, respectively. Scale bars, 10 μm.

(B) Co-expression of PLVCub-*At*CNIH5 with NubG-*At*PHF1, NubG-*At*PHT1;1, and NubG-*At*PHT1;4 in the yeast split-ubiquitin system. The co-expression of PLVCub-*At*CNIH5 with NubWT and NubG are used as positive and negative controls, respectively. Yeast transformants were grown on synthetic medium without leucine and tryptophan (–LW; the left panel) or on synthetic medium lacking leucine, tryptophan, adenine, and histidine-containing 500 μM methionine (–LWAH; middle panel) or on SC–LW containing 2 mg/L X-gal (X-gal; the right panel).

(C) Coimmunoprecipitation of *At*PHT1;1/2/3 with GFP-*AtCNIH5* in *UBQ10*: GFP and *AtCNIH5pro*: GFP-*AtCNIH5/cnih5* complementation (COM) 11-day-old seedlings grown under Pi-deficient (–P, 0 μM KH_2PO_4, seven days of starvation) conditions. The amount of root low-speed pellet (LSP) membrane fraction used for the input or the immunoprecipitation (IP) loading was shown as indicated. The relative expression was normalized with the corresponding control.

Figure 4. Loss of *AtCNIH5* leads to decreased shoot Pi levels, lower abundance of *At*PHT1 proteins, and diminished Pi uptake.

(A and B) The shoot and root fresh weight (FW) (A) and Pi levels (B) of 11-day-old seedlings of *Arabidopsis* WT and *cnih5* under Pi-sufficient (+P, 250 μM KH_2PO_4) and Pi-deficient (–P, 0 μM KH_2PO_4, three days of starvation) conditions. Error bars represent SE (n = 15–16,

pools of seedlings from independent experiments; $^{*}P < 0.05$, $^{**}P < 0.01$; Student's t-test, two-tailed).

(C) Expression of *At*PHT1;1/2/3 and *At*PHT1;4 in the root microsomal fractions from 11-day-old *Arabidopsis* WT and *cnih5* seedlings under Pi-sufficient (+P, 250 μM KH_2PO_4) and Pi-deficient (–P, 0 μM KH_2PO_4, three days of starvation) conditions. The relative expression level of *At*PHT1;1/2/3 and *At*PHT1;4 was normalized with the corresponding amido black staining and relative to the WT control. Error bars represent SE (n = 2, pools of seedlings from independent experiments)

(D) Quantification of Pi uptake and shoot-to-root distribution. Data are visualized using BoxPlotR (Spitzer et al., 2014). The center lines show the medians; the central plus signs (+) show the means; box limits indicate the 25th and 75th percentiles; whiskers extend to the minimum and the maximum values. Data points are plotted as dots. Data significantly different from WT are indicated by asterisks (n = 8 biological replicates; $^{*}P < 0.05$, $^{**}P < 0.01$; Student's t-test, two-tailed).

Figure 5. Impaired plasma membrane targeting of split-GFP-tagged *At*PHT1;1 in *cnih5* root.

(A) Reduction of *At*PHT1;1-S11 at the plasma membrane of the epidermal cells in the root transition/elongation zone of 5-day-old *cnih5* seedlings under Pi-deficient (−P, 0 μM KH_2PO_4) conditions. The transgenic lines expressing *AtPHT1;1pro*: *At*PHT1;1-S11/*35S*: GFP1–10 in the *cnih5* and corresponding WT backgrounds were used for comparison. Representative images and line-scan profiles of fluorescence intensity (arbitrary unit, a.u.) of *At*PHT1;1-S11 were shown in the left panel. Arrows indicate the acropetal direction. In the right panel, fluorescence intensity histogram of *At*PHT1;1-S11 enclosed by the representative rectangular is used for quantification. Data significantly different from WT are indicated by asterisks (n = 49 or 48 regions from transition/elongation zone of 8 roots; $^{**}P < 0.01$; Student's t-test, two-tailed). Scale bars, 20 μm.

(B) Representative image showing increased intracellular retention of *At*PHT1;1-S11 in the root epidermal cells along the transition/elongation zone of *cnih5*. Scale bars, 20 μm.

(C) Reduction of *At*PHT1;1-S11 at the plasma membrane in the *cnih5* root hair. Line-scan

profiles of fluorescence intensity (arbitrary unit, a.u.) of *At*PHT1;1-S11 were performed as indicated by the dash line at a distance of 30 μm from the root hair tip in the left panel. Quantitative data were shown in the right panel. The center lines show the medians; the central plus signs (+) show the means; box limits indicate the 25th and 75th percentiles; whiskers extend to the smallest data point within 1.5 times the interquartile range from the lower and upper quartiles. Data points are plotted as dots. Data significantly different from WT are indicated by asterisks (n = 21 or 30 root hairs; $^{**}P < 0.01$; Student's t-test, two-tailed). Scale bars, 20 μm.

Figure 6. Loss of *AtCNIH5* exacerbates the growth retardation of *phf1*.

(A and B) The shoot and root fresh weight (FW) (A) and Pi levels (B) of 11-day-old seedlings of *Arabidopsis* WT, *phf1, phf1/cnih4, phf1/cnih5*, and *phf1/cnih4/5* grown under Pi-sufficient (+P, 250 μM KH_2PO_4) and Pi-deficient (–P, 0 μM KH_2PO_4, three days of starvation) conditions. Error bars represent SE (n = 7–8, pools of seedlings from independent experiments; $^{*}P < 0.05$, $^{**}P < 0.01$; Student's t-test, two-tailed).

(C) The expression of *At*PHT1;1/2/3 in the root of 11-day-old *Arabidopsis* WT, *phf1, phf1/cnih4, phf1/cnih5*, and *phf1/cnih4/5* seedlings grown under Pi-sufficient (+P, 250 μM KH_2PO_4) and Pi-deficient (–P, 0 μM KH_2PO_4, three days of starvation) conditions. The relative expression level of *At*PHT1;1/2/3 was normalized with the corresponding actin and relative to the WT control. Error bars represent SE (n = 3, pools of seedlings from independent experiments).

Figure 7. Loss of *AtCNIH5* suppresses Pi accumulation in *Arabidopsis pho2*.

(A and B) The shoot Pi level (A) and the expression of *At*PHT1;1/2/3, *At*PHT1;4 and *At*PHO1 in the root (B) of 11-day-old *Arabidopsis* WT, *pho2,* and *cnih5/pho2* seedlings grown under Pi-sufficient (+P, 250 μM KH_2PO_4) conditions. Error bars represent SE (n = 5–7, pools of seedlings from independent experiments; WT or *cnih5/pho2* versus *pho2*, $^{**}P < 0.01$; Student's t-test, two-tailed). One representative immunoblot from two independent experiments is shown.

Figure 8. A working model of *At*CNIH5-mediated ER exit of *At*PHT1s.

In *Arabidopsis*, *PHF1* and *CNIH5* are expressed at distinct and overlapping root developmental zones (left panel). In the non-dividing epidermal cell (right panel), including the transition zone/elongation zone and the root hair cell of the differentiation zone, the transcripts of *PHT1* genes, *PHF1*, and *CNIH5* are increased under Pi starvation (−P). CNIH5 interacts with PHF1 to facilitate the ER exit and the plasma membrane (PM) targeting of PHT1s in a COPII-dependent manner. While PHF1 may interact with PHT1s that are competent for the ER exit at an upstream step of COPII recruitment, CNIH5 may selectively mediate the efficient incorporation of PHT1s into the COPII vesicle delivered to the Golgi. CNIH5 may also acts as a cargo receptor for other membrane proteins. RAM, root apical meristem; TZ, transition zone; EZ, elongation zone, DZ, differentiation zone.

Table 1. Intracellular retention of *At*PHT1;1 in the root transition/elongation zones of *cnih5*.

REFERENCES

Ames, B.N. (1966). [10] Assay of inorganic phosphate, total phosphate and phosphatases. In Methods in enzymology (Elsevier), pp. 115-118.

Ayadi, A., David, P., Arrighi, J.-F., Chiarenza, S., Thibaud, M.-C., Nussaume, L., and Marin, E. (2015). Reducing the Genetic Redundancy of Arabidopsis PHOSPHATE TRANSPORTER1 Transporters to Study Phosphate Uptake and Signaling Plant Physiology **167,** 1511-1526.

Bayle, V., Arrighi, J.-F., Creff, A., Nespoulous, C., Vialaret, J., Rossignol, M., Gonzalez, E., Paz-Ares, J., and Nussaume, L. (2011). Arabidopsis thaliana High-Affinity Phosphate Transporters Exhibit Multiple Levels of Posttranslational Regulation. The Plant Cell **23,** 1523-1535.

Bökel, C., Dass, S., Wilsch-Bräuninger, M., and Roth, S. (2006). Drosophila Cornichon acts as cargo receptor for ER export of the TGFα-like growth factor Gurken. Development **133,** 459-470.

Cardona-López, X., Cuyas, L., Marín, E., Rajulu, C., Irigoyen, M.L., Gil, E., Puga, M.I., Bligny, R., Nussaume, L., and Geldner, N. (2015). ESCRT-III-associated protein ALIX mediates high-affinity phosphate transporter trafficking to maintain phosphate homeostasis in Arabidopsis. The Plant Cell **27,** 2560-2581.

Chen, J., Wang, Y., Wang, F., Yang, J., Gao, M., Li, C., Liu, Y., Liu, Y., Yamaji, N., Ma, J.F., Paz-Ares, J., Nussaume, L., Zhang, S., Yi, K., Wu, Z., and Wu, P. (2015). The Rice CK2 Kinase Regulates Trafficking of Phosphate Transporters in Response to Phosphate Levels. The Plant Cell **27,** 711-723.

Clough, S.J., and Bent, A.F. (1998). Floral dip: a simplified method for Agrobacterium-mediated transformation of Arabidopsis thaliana. The plant journal **16,** 735-743.

Delhaize, E., and Randall, P.J. (1995). Characterization of a phosphate-accumulator mutant of Arabidopsis thaliana. Plant Physiology **107,** 207-213.

Gahoonia, T.S., and Nielsen, N.E. (1998). Direct evidence on participation of root hairs in phosphorus (32P) uptake from soil. Plant and Soil **198,** 147-152.

González, E., Solano, R., Rubio, V., Leyva, A., and Paz-Ares, J. (2005). PHOSPHATE TRANSPORTER TRAFFIC FACILITATOR1 Is a Plant-Specific SEC12-Related Protein That Enables the Endoplasmic Reticulum Exit of a High-Affinity Phosphate Transporter in *Arabidopsis*. The Plant Cell **17,** 3500-3512.

Harmel, N., Cokic, B., Zolles, G., Berkefeld, H., Mauric, V., Fakler, B., Stein, V., and Klöcker, N. (2012). AMPA receptors commandeer an ancient cargo exporter for use as an auxiliary subunit for signaling. PloS one **7,** e30681-e30681.

Herzig, Y., Sharpe, H.J., Elbaz, Y., Munro, S., and Schuldiner, M. (2012). A Systematic Approach to Pair Secretory Cargo Receptors with Their Cargo Suggests a Mechanism for Cargo Selection by Erv14. PLOS Biology **10,** e1001329.

Huang, T.-K., Han, C.-L., Lin, S.-I., Chen, Y.-J., Tsai, Y.-C., Chen, Y.-R., Chen, J.-W., Lin, W.-Y., Chen, P.-M., Liu, T.-Y., Chen, Y.-S., Sun, C.-M., and Chiou, T.-J. (2013). Identification of Downstream Components of Ubiquitin-Conjugating Enzyme PHOSPHATE2 by Quantitative Membrane Proteomics in Arabidopsis Roots. The Plant Cell **25,** 4044-4060.

Jones Alexander, M., Xuan, Y., Xu, M., Wang, R.-S., Ho, C.-H., Lalonde, S., You Chang, H., Sardi Maria, I., Parsa Saman, A., Smith-Valle, E., Su, T., Frazer Keith, A., Pilot, G., Pratelli, R., Grossmann, G., Acharya Biswa, R., Hu, H.-C., Engineer, C., Villiers, F., Ju, C., Takeda, K., Su, Z., Dong, Q., Assmann Sarah, M., Chen, J., Kwak June, M., Schroeder Julian, I., Albert, R., Rhee Seung, Y., and Frommer Wolf, B. (2014). Border Control—A Membrane-Linked Interactome of Arabidopsis. Science **344,** 711-716.

Kanno, S., Arrighi, J.-F., Chiarenza, S., Bayle, V., Berthome, R., Peret, B., Javot, H., Delannoy, E., Marin, E., and Nakanishi, T.M. (2016). A novel role for the root cap in phosphate uptake and homeostasis. Elife **5,** e14577.

Karthikeyan, A.S., Varadarajan, D.K., Mukatira, U.T., D'Urzo, M.P., Damsz, B., and Raghothama, K.G. (2002). Regulated Expression of Arabidopsis Phosphate Transporters. Plant Physiology **130,** 221-233.

Lambers, H., Raven, J.A., Shaver, G.R., and Smith, S.E. (2008). Plant nutrient-acquisition strategies change with soil age. Trends in Ecology & Evolution **23,** 95-103.

Lau, W.-T.W., Howson, R.W., Malkus, P., Schekman, R., and O'Shea, E.K. (2000). Pho86p, an endoplasmic reticulum (ER) resident protein in Saccharomyces cerevisiae, is required for ER exit of the high-affinity phosphate transporter Pho84p. Proceedings of the National Academy of Sciences **97,** 1107-1112.

Li, X. (2011). Histostaining for tissue expression pattern of promoter-driven GUS activity in Arabidopsis. Bio-protocol, e93-e93.

Liebminger, E., Huttner, S., Vavra, U., Fischl, R., Schoberer, J., Grass, J., Blaukopf, C., Seifert, G.J., Altmann, F., and Mach, L. (2009). Class I α-mannosidases are required for N-glycan processing and root development in Arabidopsis thaliana. The

Plant Cell **21,** 3850-3867.
Lin, W.-Y., Huang, T.-K., and Chiou, T.-J. (2013). Nitrogen limitation adaptation, a target of microRNA827, mediates degradation of plasma membrane-localized phosphate transporters to maintain phosphate homeostasis in Arabidopsis. The Plant cell **25,** 4061-4074.
Liu, T.-Y. (2021). Using Tripartite Split-sfGFP for the Study of Membrane Protein–Protein Interactions. In Arabidopsis Protocols, J.J. Sanchez-Serrano and J. Salinas, eds (New York, NY: Springer US), pp. 323-336.
Liu, T.-Y., Chou, W.-C., Chen, W.-Y., Chu, C.-Y., Dai, C.-Y., and Wu, P.-Y. (2018). Detection of membrane protein–protein interaction in planta based on dual-intein-coupled tripartite split-GFP association. The Plant Journal **94,** 426-438.
Liu, T.-Y., Tsai, M.-H., Wang, J.-Y., Lung, H.-F., Chow, H.-X., Chiu, C.-Y., and Lu, C.-A. (2024). CORNICHON HOMOLOG 5-dependent ER export of membrane cargoes in phosphate-starved Arabidopsis root as revealed by membrane proteomic analysis. bioRxiv**,** 2024.2012.2030.630708.
Liu, T.-Y., Huang, T.-K., Tseng, C.-Y., Lai, Y.-S., Lin, S.-I., Lin, W.-Y., Chen, J.-W., and Chiou, T.-J. (2012). PHO2-Dependent Degradation of PHO1 Modulates Phosphate Homeostasis in Arabidopsis The Plant Cell **24,** 2168-2183.
Liu, T.-Y., Huang, T.-K., Yang, S.-Y., Hong, Y.-T., Huang, S.-M., Wang, F.-N., Chiang, S.-F., Tsai, S.-Y., Lu, W.-C., and Chiou, T.-J. (2016). Identification of plant vacuolar transporters mediating phosphate storage. Nature Communications **7,** 11095.
Müller, R., Morant, M., Jarmer, H., Nilsson, L., and Nielsen, T.H. (2007). Genome-Wide Analysis of the Arabidopsis Leaf Transcriptome Reveals Interaction of Phosphate and Sugar Metabolism. Plant Physiology **143,** 156-171.
Manning, D.A.C. (2008). Phosphate Minerals, Environmental Pollution and Sustainable Agriculture. Elements **4,** 105-108.
Misson, J., Thibaud, M.-C., Bechtold, N., Raghothama, K., and Nussaume, L. (2004). Transcriptional regulation and functional properties of Arabidopsis Pht1; 4, a high affinity transporter contributing greatly to phosphate uptake in phosphate deprived plants. Plant molecular biology **55,** 727-741.
Młodzińska, E., and Zboińska, M. (2016). Phosphate Uptake and Allocation – A Closer Look at Arabidopsis thaliana L. and Oryza sativa L. Frontiers in Plant Science **7**.
Mudge, S.R., Rae, A.L., Diatloff, E., and Smith, F.W. (2002). Expression analysis suggests novel roles for members of the Pht1 family of phosphate transporters in Arabidopsis. The Plant Journal **31,** 341-353.
Nakanishi, H., Suda, Y., and Neiman, A.M. (2007). Erv14 family cargo receptors are necessary for ER exit during sporulation in Saccharomyces cerevisiae. Journal of Cell Science **120,** 908-916.
Nelson, B.K., Cai, X., and Nebenführ, A. (2007). A multicolored set of in vivo organelle markers for co-localization studies in Arabidopsis and other plants. The Plant Journal **51,** 1126-1136.
Obrdlik, P., El-Bakkoury, M., Hamacher, T., Cappellaro, C., Vilarino, C., Fleischer, C., Ellerbrok, H., Kamuzinzi, R., Ledent, V., Blaudez, D., Sanders, D., Revuelta, J.L., Boles, E., André, B., and Frommer, W.B. (2004). K+ channel interactions

detected by a genetic system optimized for systematic studies of membrane protein interactions. Proceedings of the National Academy of Sciences of the United States of America **101,** 12242-12247.

Pagant, S., Wu, A., Edwards, S., Diehl, F., and Miller, Elizabeth A. (2015). Sec24 Is a Coincidence Detector that Simultaneously Binds Two Signals to Drive ER Export. Current Biology **25,** 403-412.

Park, B.S., Seo, J.S., and Chua, N.-H. (2014). NITROGEN LIMITATION ADAPTATION Recruits PHOSPHATE2 to Target the Phosphate Transporter PT2 for Degradation during the Regulation of Arabidopsis Phosphate Homeostasis. The Plant Cell **26,** 454-464.

Poirier, Y., and Bucher, M. (2002). Phosphate Transport and Homeostasis in Arabidopsis. The Arabidopsis Book, e0024.

Powers, J., and Barlowe, C. (1998). Transport of Axl2p Depends on Erv14p, an ER–Vesicle Protein Related to the Drosophila cornichon Gene Product. The Journal of Cell Biology **142,** 1209-1222.

Powers, J., and Barlowe, C. (2002). Erv14p Directs a Transmembrane Secretory Protein into COPII-coated Transport Vesicles. Molecular Biology of the Cell **13,** 880-891.

Rosas-Santiago, P., Lagunas-Gómez, D., Barkla, B.J., Vera-Estrella, R., Lalonde, S., Jones, A., Frommer, W.B., Zimmermannova, O., Sychrová, H., and Pantoja, O. (2015). Identification of rice cornichon as a possible cargo receptor for the Golgi-localized sodium transporter OsHKT1;3. Journal of Experimental Botany **66,** 2733-2748.

Roth, S., Shira Neuman-Silberberg, F., Barcelo, G., and Schüpbach, T. (1995). cornichon and the EGF receptor signaling process are necessary for both anterior-posterior and dorsal-ventral pattern formation in Drosophila. Cell **81,** 967-978.

Schlücking, K., Edel, K.H., Köster, P., Drerup, M.M., Eckert, C., Steinhorst, L., Waadt, R., Batistič, O., and Kudla, J. (2013). A new β-estradiol-inducible vector set that facilitates easy construction and efficient expression of transgenes reveals CBL3-dependent cytoplasm to tonoplast translocation of CIPK5. Molecular plant **6,** 1814-1829.

Schneider, C.A., Rasband, W.S., and Eliceiri, K.W. (2012). NIH Image to ImageJ: 25 years of image analysis. Nature Methods **9,** 671-675.

Shahan, R., Hsu, C.-W., Nolan, T.M., Cole, B.J., Taylor, I.W., Greenstreet, L., Zhang, S., Afanassiev, A., Vlot, A.H.C., Schiebinger, G., Benfey, P.N., and Ohler, U. (2022). A single-cell Arabidopsis root atlas reveals developmental trajectories in wild-type and cell identity mutants. Developmental Cell **57,** 543-560.e549.

Shin, H., Shin, H.-S., Dewbre, G.R., and Harrison, M.J. (2004). Phosphate transport in Arabidopsis: Pht1;1 and Pht1;4 play a major role in phosphate acquisition from both low- and high-phosphate environments. The Plant Journal **39,** 629-642.

Spitzer, M., Wildenhain, J., Rappsilber, J., and Tyers, M. (2014). BoxPlotR: a web tool for generation of box plots. Nature methods **11,** 121-122.

Takagi, J., Renna, L., Takahashi, H., Koumoto, Y., Tamura, K., Stefano, G., Fukao, Y., Kondo, M., Nishimura, M., Shimada, T., Brandizzi, F., and Hara-Nishimura, I. (2013). MAIGO5 Functions in Protein Export from Golgi-Associated Endoplasmic Reticulum Exit Sites in Arabidopsis The Plant Cell **25,** 4658-4675.

Tanaka, N., Kato, M., Tomioka, R., Kurata, R., Fukao, Y., Aoyama, T., and Maeshima, M. (2014). Characteristics of a root hair-less line of Arabidopsis thaliana under physiological stresses. Journal of Experimental Botany **65,** 1497-1512.

Trevor, M.N., Nemanja, V., Che-Wei, H., Jingyuan, Z., Isabelle, V., Rachel, S., Isaiah, W.T., Laura, G., Matthieu, H., Ping, W., Pablo, S., Aiden, B., Yanhai, Y., Geoffrey, S., Uwe, O., Eugenia, R., and Philip, N.B. (2022). Brassinosteroid gene regulatory networks at cellular resolution. bioRxiv**,** 2022.2009.2016.508001.

Wei, L., Liu, L., Chen, Z., Huang, Y., Yang, L., Wang, P., Xue, S., and Bie, Z. (2023). CmCNIH1 improves salt tolerance by influencing the trafficking of CmHKT1;1 in pumpkin. The Plant Journal **114,** 1353-1368.

Wudick, M.M., Portes, M.T., Michard, E., Rosas-Santiago, P., Lizzio, M.A., Nunes, C.O., Campos, C., Santa Cruz Damineli, D., Carvalho, J.C., Lima, P.T., Pantoja, O., and Feijó, J.A. (2018). CORNICHON sorting and regulation of GLR channels underlie pollen tube Ca2+ homeostasis. Science **360,** 533-536.

Yang, Z., Yang, J., Wang, Y., Wang, F., Mao, W., He, Q., Xu, J., Wu, Z., and Mao, C. (2020). PROTEIN PHOSPHATASE95 Regulates Phosphate Homeostasis by Affecting Phosphate Transporter Trafficking in Rice. The Plant Cell **32,** 740.

Yáñez-Domínguez, C., Lagunas-Gómez, D., Torres-Cifuentes, D.M., Bezanilla, M., and Pantoja, O. (2023). A cornichon protein controls polar localization of the PINA auxin transporter in Physcomitrium patens. Development **150,** dev201635.

Yoshimoto, K., Hanaoka, H., Sato, S., Kato, T., Tabata, S., Noda, T., and Ohsumi, Y. (2004). Processing of ATG8s, ubiquitin-like proteins, and their deconjugation by ATG4s are essential for plant autophagy. The Plant cell **16,** 2967-2983.

Zimmermannová, O., Felcmanová, K., Rosas-Santiago, P., Papoušková, K., Pantoja, O., and Sychrová, H. (2019). Erv14 cargo receptor participates in regulation of plasma-membrane potential, intracellular pH and potassium homeostasis via its interaction with K+-specific transporters Trk1 and Tok1. Biochimica et Biophysica Acta (BBA) - Molecular Cell Research **1866,** 1376-1388.

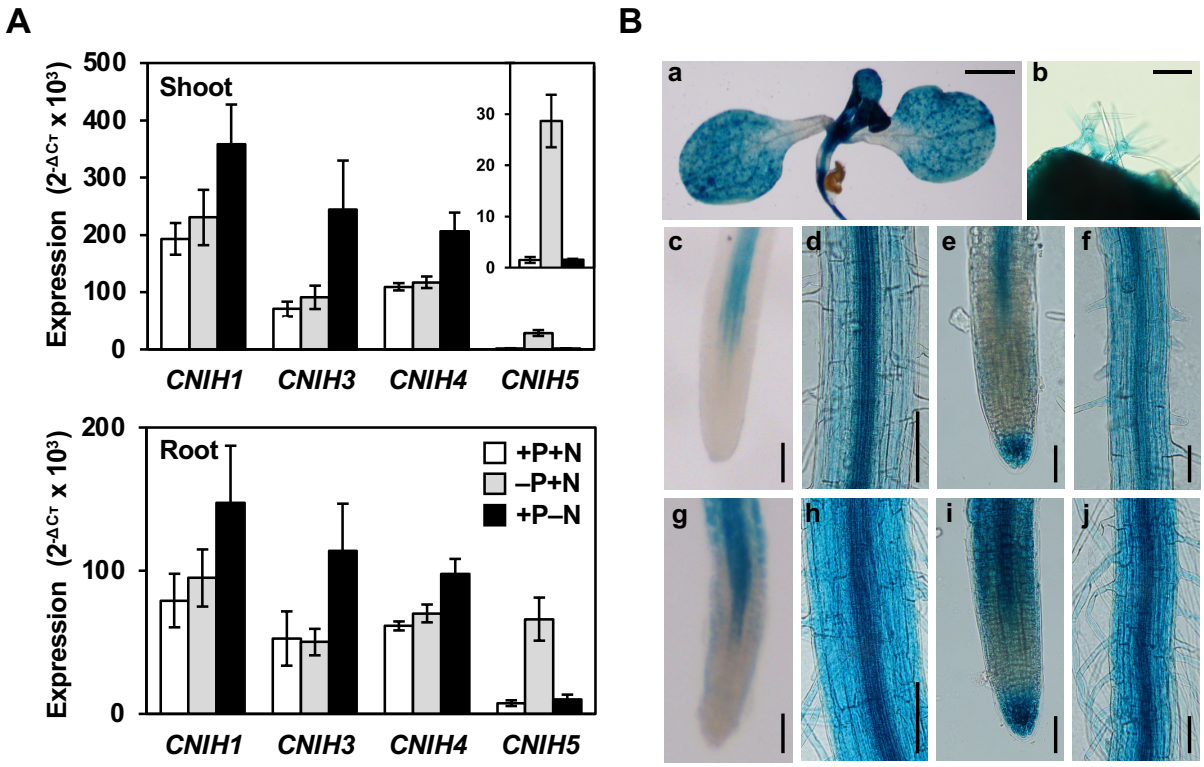

Figure 1. Pi starvation-induced expression pattern of *At*CNIH5.

(A) RT-qPCR analysis of *A. thaliana CNIH1, CNIH3, CNIH4,* and *CNIH5* in the shoot and root of 11-day-old seedlings grown under full nutrient (+P+N, 250 μM KH_2PO_4 and 7.5 mM KNO_3), Pi-deficient (–P+N, 0 μM KH_2PO_4 and 7.5 mM KNO_3, three days of starvation) and N-deficient (+P–N, 250 μM KH_2PO_4 and 0 μM KNO_3, three days of starvation) conditions. The magnified inset on the right top shows low Pi induction of *AtCNIH5* in the shoot. Error bars represent SE (n = 3, pools of seedings from independent experiments).

(B) Expression of *AtCNIH5pro*: GUS in 7-day-old seedlings grown under Pi-sufficient (+P, 250 μM KH_2PO_4) and Pi-deficient (–P, 0 μM KH_2PO_4, five days of starvation) conditions. a–f (+P; shoot part; trichome; primary root tip; primary root maturation zone; lateral root tip; lateral root maturation zone). g–j (–P; root tip; primary root maturation zone; lateral root tip; lateral root maturation zone). Scale bars, 10 mm in a, 0.1 mm in b, and 100 μm in c–j.

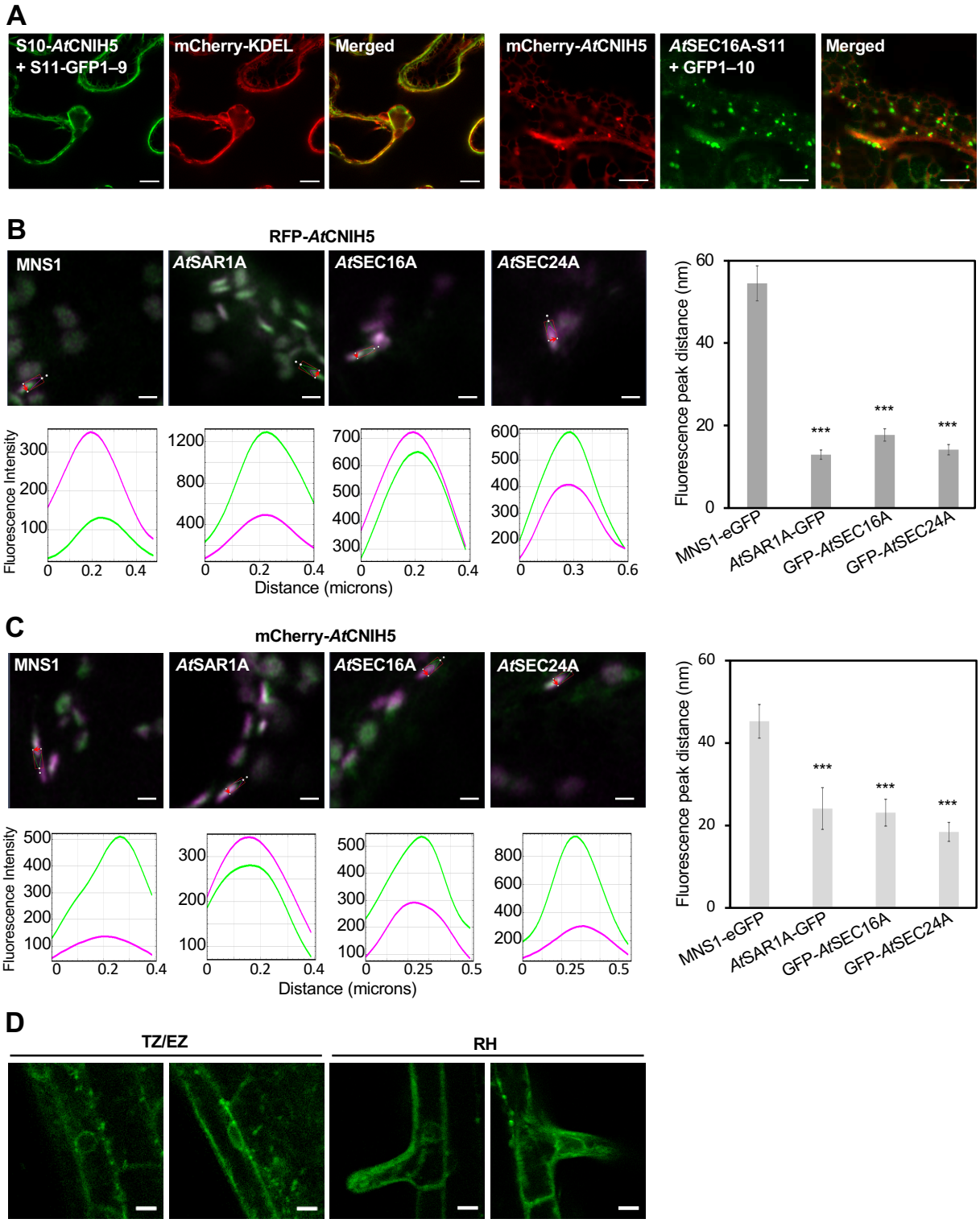

Figure 2. Subcellular localization of *At*CNIH5 to the ER and ERES.

(A) The ER and ERES localizations of S10-*At*CNIH5 in agro-infiltrated *N. benthamiana* leaves. mCherry-HDEL, luminal ER marker; *At*SEC16A-S11, ERES marker. Scale bars, 10 μm.

(B and C) Statistical line profile analysis of fluorescence intensity for localization of *At*CNIH5 with the ERES and *cis*-Golgi markers. Representative images and line profile analysis for RFP-*At*CNIH5 (B) and mCherry-*At*CNIH5 (C) (magenta) with the *cis*-Golgi marker MNS1-eGFP and the ERES markers *At*SAR1A-GFP, GFP-*At*SEC16A, and GFP-*At*SEC24A (green). Line profile applied and line profile output are shown. Peak distance analysis graphs showing the co-localization analysis with RFP-*At*CNIH5 and mCherry-*At*CNIH5 with the ERES and *cis*-Golgi markers. Scale bars = 1 μm. Significance was analyzed by Kruskal–Wallis (***$P < 0.001$). Error bars represent SE (n = 4 biological replicas, with at least 18 technical repeats).

(D) Localization of GFP-*AtCNIH5* in the root of *Arabidopsis* 5-day-old seedlings grown under Pi-deficient (–P, 0 μM KH_2PO_4, five days of starvation) conditions. TZ/EZ, transition zone/elongation zone; RH, root hair. Scale bars, 10 μm.

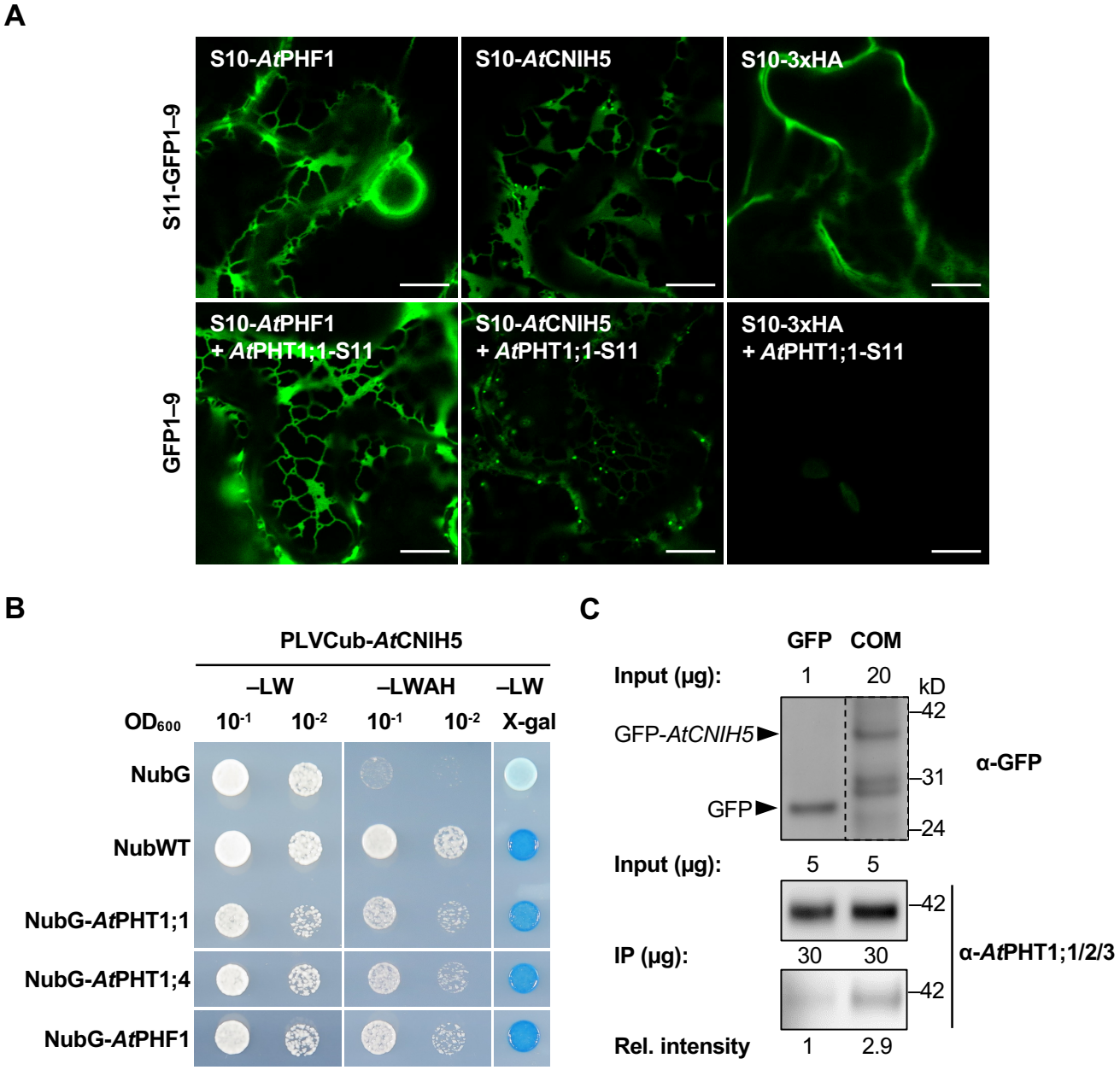

Figure 3. *At*CNIH5 interacts with *At*PHT1;1, *At*PHT1;4, and *At*PHF1.

(A) Expression of S10-*At*CNIH5, S10-*At*PHF1, S10-3xHA and *At*PHT1;1-S11 in the presence of S11-GFP1–9 or GFP1–9 in *N. benthamiana* leaves. The co-expression of *At*PHT1;1-S11 with S10-*At*PHF1 and S10-3xHA are used as positive and negative protein–protein interaction controls, respectively. Scale bars, 10 μm.

(B) Co-expression of PLVCub-*At*CNIH5 with NubG-*At*PHF1, NubG-*At*PHT1;1, and NubG-*At*PHT1;4 in the yeast split-ubiquitin system. The co-expression of PLVCub-*At*CNIH5 with NubWT and NubG are used as positive and negative controls, respectively. Yeast transformants were grown on synthetic medium without leucine and tryptophan (–LW; the left panel) or on synthetic medium lacking leucine, tryptophan, adenine, and histidine-containing 500 μM methionine (–LWAH; middle panel) or on SC–LW containing 2 mg/L X-gal (X-gal; the right panel).

(C) Coimmunoprecipitation of *At*PHT1;1/2/3 with GFP-*AtCNIH5* in *UBQ10*: GFP and *AtCNIH5pro*: GFP-*AtCNIH5/cnih5* complementation (COM) 11-day-old seedlings grown under Pi-deficient (–P, 0 μM KH_2PO_4, seven days of starvation) conditions. The amount of root low-speed pellet (LSP) membrane fraction used for the input or the immunoprecipitation (IP) loading was shown as indicated. The relative expression was normalized with the corresponding control.

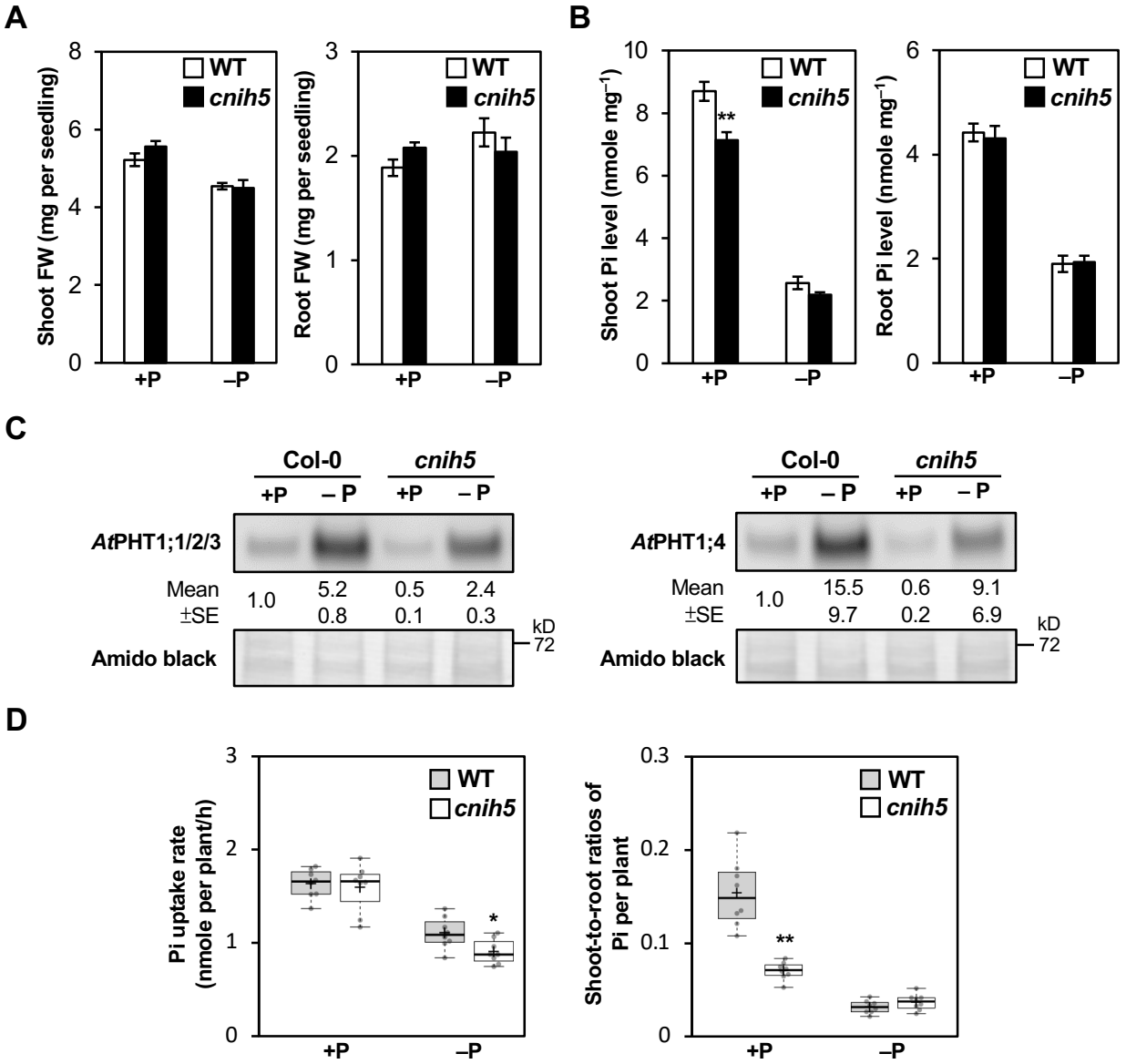

Figure 4. Loss of *AtCNIH5* leads to decreased shoot Pi levels, lower abundance of *At*PHT1 proteins, and diminished Pi uptake.

(A and B) The shoot and root fresh weight (FW) (A) and Pi levels (B) of 11-day-old seedlings of *Arabidopsis* WT, *cnih4*, and *cnih5* under Pi-sufficient (+P, 250 μM KH_2PO_4) and Pi-deficient (–P, 0 μM KH_2PO_4, three days of starvation) conditions. Error bars represent SE (n = 15–16, pools of seedlings from independent experiments; $^{*}P < 0.05$, $^{**}P < 0.01$; Student's t-test, two-tailed).

(C) Expression of *At*PHT1;1/2/3 and *At*PHT1;4 in the root microsomal fractions from 11-day-old *Arabidopsis* WT and *cnih5* seedlings under Pi-sufficient (+P, 250 μM KH_2PO_4) and Pi-deficient (–P, 0 μM KH_2PO_4, three days of starvation) conditions. The relative expression level of *At*PHT1;1/2/3 and *At*PHT1;4 was normalized with the corresponding amido black staining and relative to the WT control. Error bars represent SE (n = 2, pools of seedlings from independent experiments)

(D) Quantification of Pi uptake and shoot-to-root distribution. Data are visualized using BoxPlotR (Spitzer et al., 2014). The center lines show the medians; the central plus signs (+) show the means; box limits indicate the 25th and 75th percentiles; whiskers extend to the minimum and the maximum values. Data points are plotted as dots. Data significantly different from WT are indicated by asterisks (n = 8 biological replicates; $^{*}P < 0.05$, $^{**}P < 0.01$; Student's t-test, two-tailed).

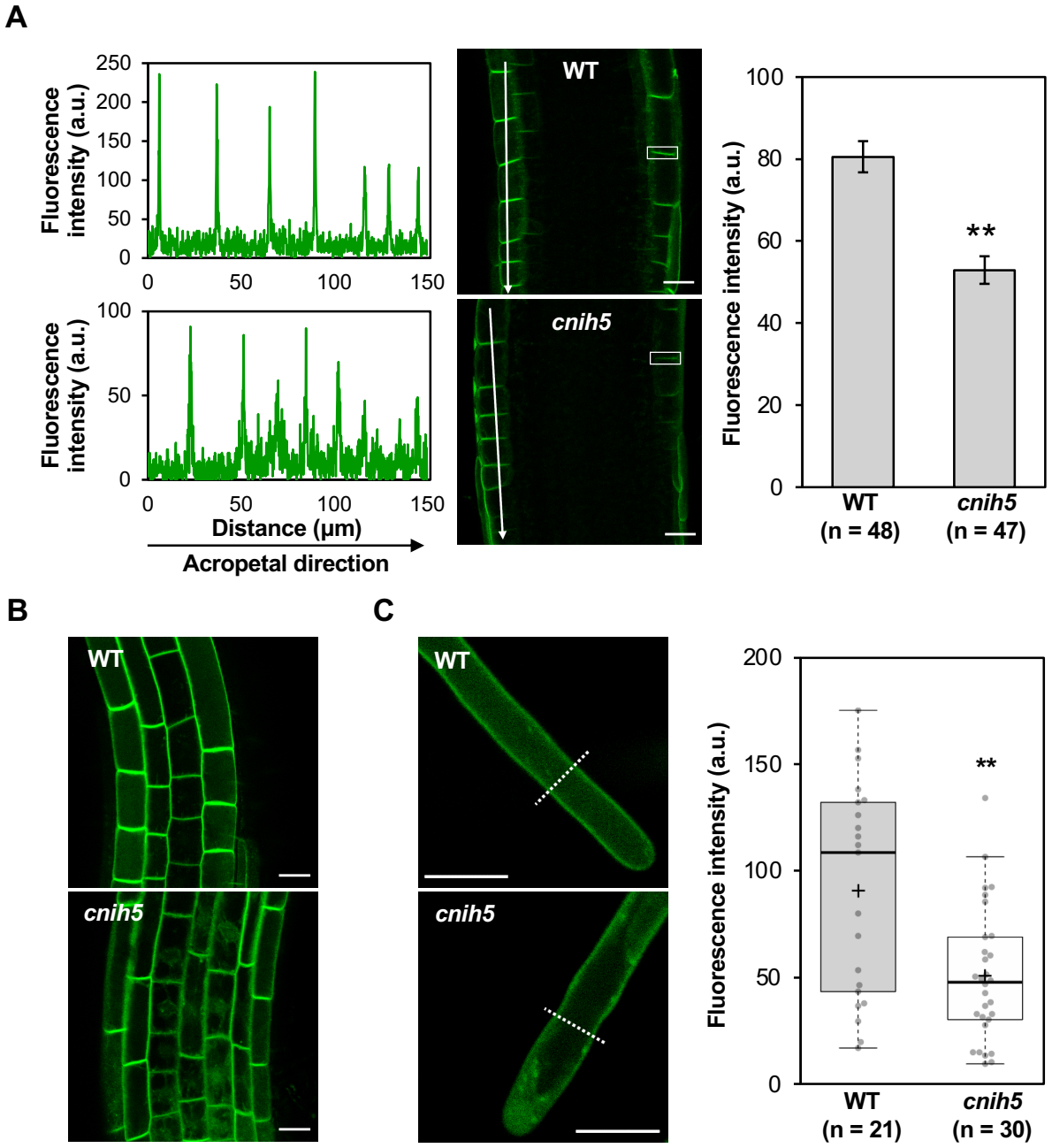

Figure 5. Impaired plasma membrane targeting of split-GFP-tagged *At*PHT1;1 in *cnih5* root.
(A) Reduction of *At*PHT1;1-S11 at the plasma membrane of the epidermal cells in the root transition/elongation zone of 5-day-old *cnih5* seedlings under Pi-deficient (−P, 0 μM KH_2PO_4) conditions. The transgenic lines expressing *AtPHT1;1pro*: *At*PHT1;1-S11/*35S*: GFP1–10 in the *cnih5* and corresponding WT backgrounds were used for comparison. Representative images and line-scan profiles of fluorescence intensity (arbitrary unit, a.u.) of *At*PHT1;1-S11 were shown in the left panel. Arrows indicate the acropetal direction. In the right panel, fluorescence intensity histogram of *At*PHT1;1-S11 enclosed by the representative rectangular is used for quantification. Data significantly different from WT are indicated by asterisks (n = 49 or 48 regions from transition/elongation zone of 8 roots; $^{**}P < 0.01$; Student's t-test, two-tailed). Scale bars, 20 μm.
(B) Representative image showing increased intracellular retention of *At*PHT1;1-S11 in the root epidermal cells along the transition/elongation zone of *cnih5*. Scale bars, 20 μm.
(C) Reduction of *At*PHT1;1-S11 at the plasma membrane in the *cnih5* root hair. Line-scan profiles of fluorescence intensity (arbitrary unit, a.u.) of *At*PHT1;1-S11 were performed as indicated by the dash line at a distance of 30 μm from the root hair tip in the left panel. Quantitative data were shown in the right panel. The center lines show the medians; the central plus signs (+) show the means; box limits indicate the 25th and 75th percentiles; whiskers extend to the smallest data point within 1.5 times the interquartile range from the lower and upper quartiles. Data points are plotted as dots. Data significantly different from WT are indicated by asterisks (n = 21 or 30 root hairs; $^{**}P < 0.01$; Student's t-test, two-tailed). Scale bars, 20 μm.

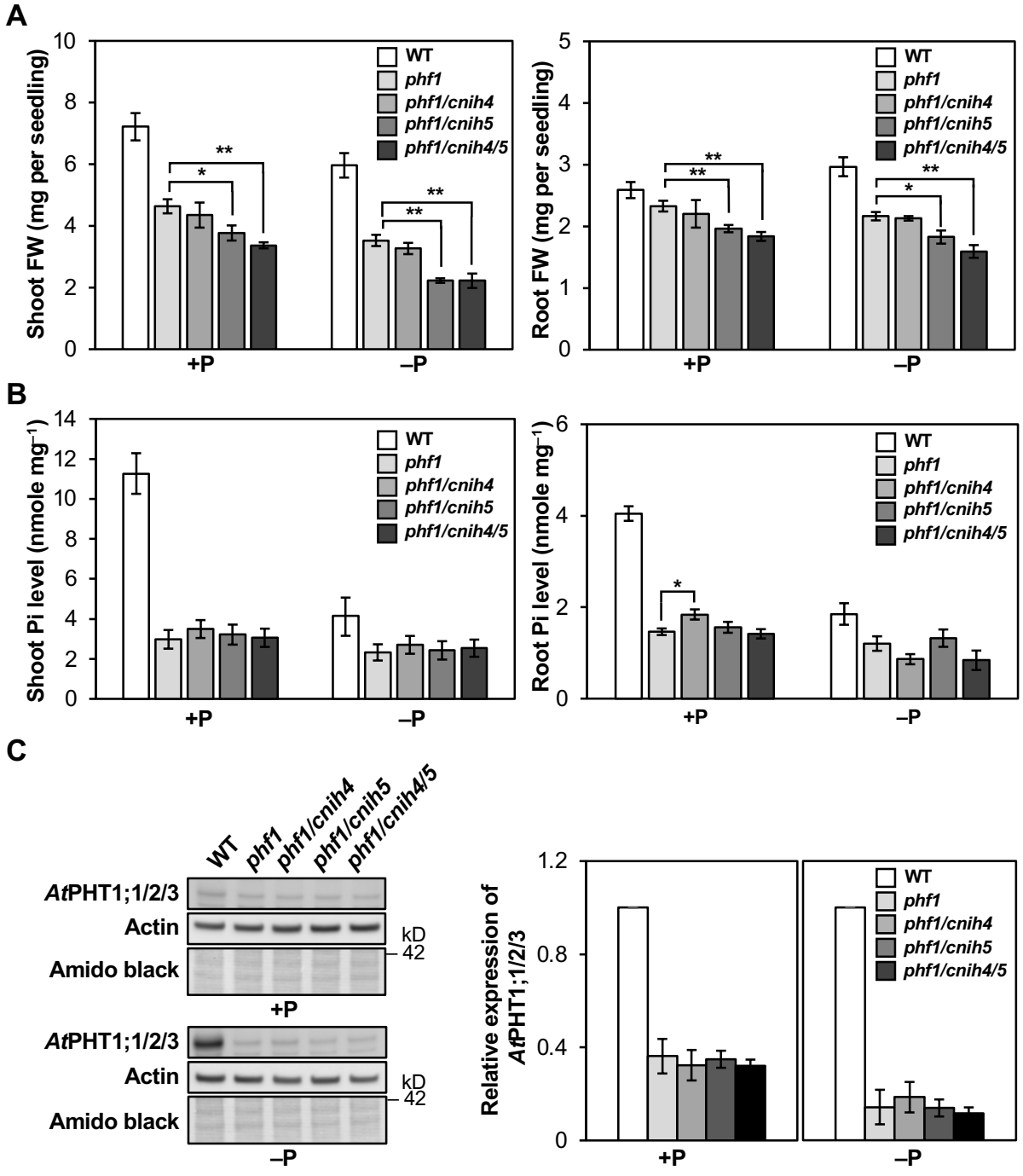

Figure 6. Loss of *AtCNIH5* exacerbates the growth retardation of *phf1*.

(A and B) The shoot and root fresh weight (FW) (A) and Pi levels (B) of 11-day-old seedlings of *Arabidopsis* WT, *phf1, phf1/cnih4, phf1/cnih5*, and *phf1/cnih4/5* grown under Pi-sufficient (+P, 250 μM KH_2PO_4) and Pi-deficient (–P, 0 μM KH_2PO_4, three days of starvation) conditions. Error bars represent SE (n = 7–8, pools of seedlings from independent experiments; $^{*}P < 0.05$, $^{**}P < 0.01$; Student's t-test, two-tailed).

(C) The expression of *At*PHT1;1/2/3 in the root of 11-day-old *Arabidopsis* WT, *phf1, phf1/cnih4, phf1/cnih5*, and *phf1/cnih4/5* seedlings grown under Pi-sufficient (+P, 250 μM KH_2PO_4) and Pi-deficient (–P, 0 μM KH_2PO_4, three days of starvation) conditions. The relative expression level of *At*PHT1;1/2/3 was normalized with the corresponding actin and relative to the WT control. Error bars represent SE (n = 3, pools of seedlings from independent experiments).

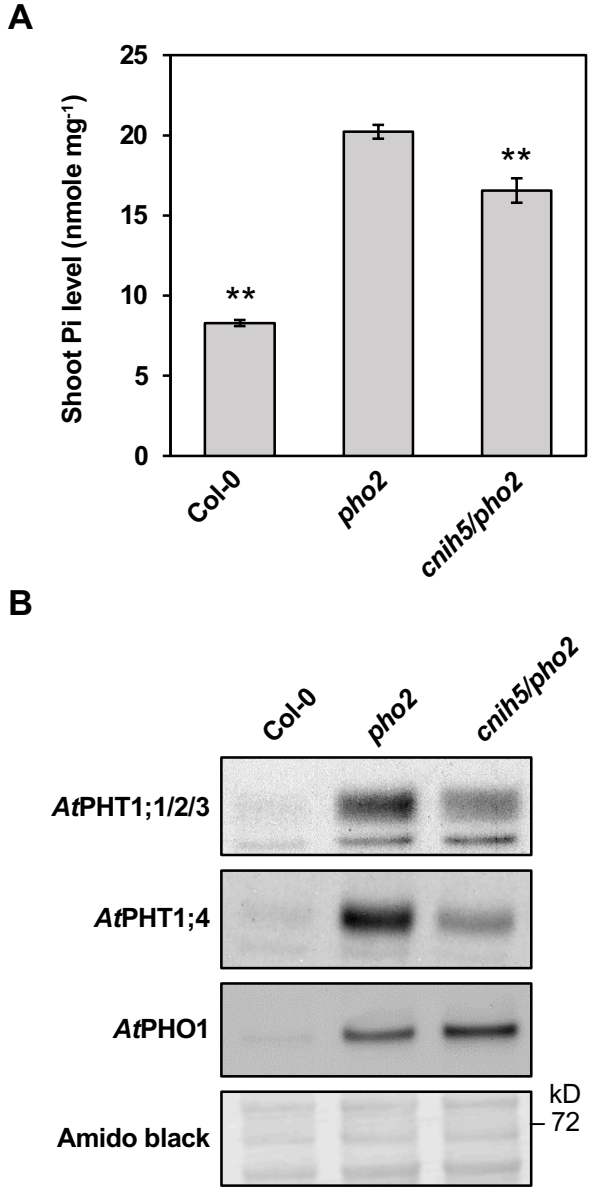

Figure 7. Loss of *AtCNIH5* suppresses Pi accumulation in *Arabidopsis pho2*.

(A and B) The shoot Pi level (A) and the expression of *At*PHT1;1/2/3, *At*PHT1;4 and *At*PHO1 in the root (B) of 11-day-old *Arabidopsis* WT, *pho2,* and *cnih5/pho2* seedlings grown under Pi-sufficient (+P, 250 μM KH_2PO_4) conditions. Error bars represent SE (n = 5–7, pools of seedlings from independent experiments; WT or *cnih5/pho2* versus *pho2*, $^{**}P < 0.01$; Student's t-test, two-tailed). One representative immunoblot from two independent experiments is shown.

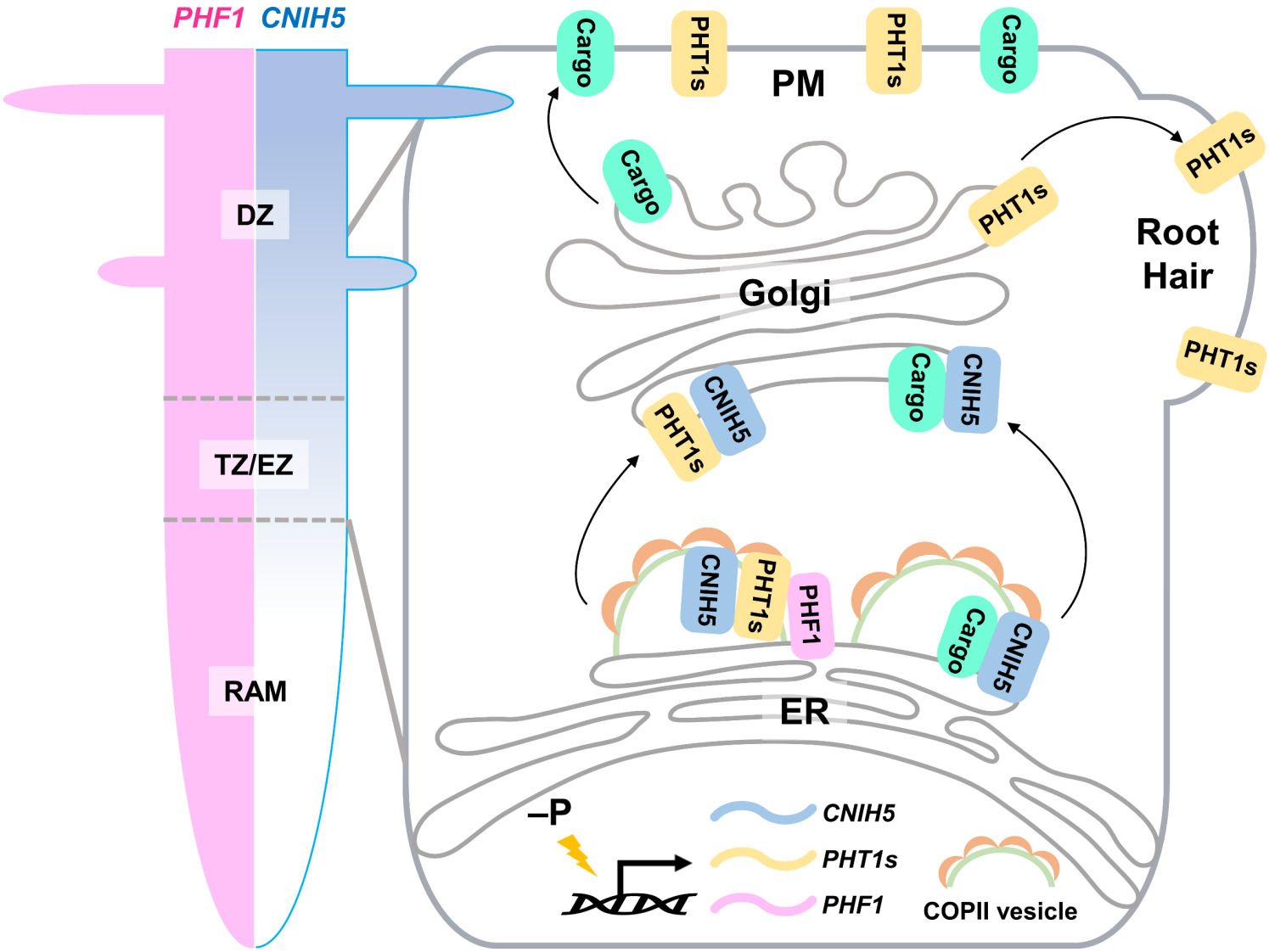

Figure 8. A working model of *At*CNIH5-mediated ER exit of *At*PHT1s.
In *Arabidopsis*, *PHF1* and *CNIH5* are expressed at distinct and overlapping root developmental zones (left panel). In the non-dividing epidermal cell (right panel), including the transition zone/elongation zone and the root hair cell of the differentiation zone, the transcripts of *PHT1* genes, *PHF1*, and *CNIH5* are increased under Pi starvation (−P). CNIH5 interacts with PHF1 to facilitate the ER exit and the plasma membrane (PM) targeting of PHT1s in a COPII-dependent manner. While PHF1 may interact with PHT1s that are competent for the ER exit at an upstream step of COPII recruitment, CNIH5 may selectively mediate the efficient incorporation of PHT1s into the COPII vesicle delivered to the Golgi. CNIH5 may also acts as a cargo receptor for other membrane proteins. RAM, root apical meristem; TZ, transition zone; EZ, elongation zone, DZ, differentiation zone.

Table 1. Intracellular retention of *At*PHT1;1 in the root transition/elongation zones of *cnih5.*

			Root 1	Root 2	Root 3	Root 4	Average (%) ± SE	*P*-value
			Number of cells displaying intracellular *At*PHT1;1-S11 divided by the number of counted cells					
TZ/EZ	Exp. 1	**WT**	0/9	0/13	5/18	1/12	9.0±6.6	<0.001
		cnih5	10/17	9/15	11/15	8/12	64.7±3.4	
	Exp. 2	**WT**	1/12	1/13	0/7	0/9	4.0±2.3	<0.001
		cnih5	7/12	4/8	7/9	5/6	67.4±7.9	

- TZ, transition zone; EZ, elongation zone.
- Exp. 1 and Exp. 2 represent two independent experiments. In each experiment, four seedlings with the WT or *cnih5* background were used for image analyses.
- Average (%) ± SE (n = 4) represents the mean and the standard error of the mean of the percentage of cells with intracellular *At*PHT1;1-S11 among counted cells.
- *P*-value is calculated based on a two-tailed Student's t-test.